Analysis of Bacterial Adhesion with Graphene Oxide-Modified PES Ultrafiltration Membranes

A THESIS SUBMITTED TO THE FACULTY OF THE UNIVERSITY OF MINNESOTA

Karl Wuolo-Journey

IN PARTIAL FULFILLMENT OF THE REQUIRMENTS FOR THE DEGREE OF MASTER OF SCIENCE

Santiago Romero-Vargas Castrillón

June 2019

Acknowledgments

I would like to thank so many people for their help finishing up this project. Firstly, I would like to thank Sara BinAhmed for her great personality, friendly conversations, insight, support, and contributions to this project (particularly, SCFS training and data analysis). I would also like to thank Elise Linna for being such a great friend as well as her contributions to the project (SCFS training and data collection). I would like to thank my advisor, Professor Santiago Romero-Vargas Castrillón, for his guidance, expertise and help with this thesis, and Professors Ray Hozalski and Chris Macosko for serving on my committee. I would like to thank Henry, John Galt, John Larkin, and Rachel for your friendship and company in the basement of the Civil Engineering building. Finally, I would like to thank my family and friends for all their support through this endeavor. I could not have done this without all of you.

Abstract

Given its potent biocidal properties, graphene oxide (GO) holds promise as a building block of anti-microbial surfaces, with numerous potential environmental applications. Nonetheless, the extent to which GO-based coatings decrease bacterial adhesion propensity, a necessary requirement of low-fouling surfaces, remains unclear. AFM-based single-cell force spectroscopy (SCFS) was used to show that coatings comprising GO nanosheets bonded to a hydrophilic polymer brush, mitigate adhesion of *Pseudomonas fluorescens* cells, while preserving GO's intrinsic biocidal activity. This work demonstrated the simultaneous biocidal and low-adhesion GO coatings by grafting poly(acrylic acid) (PAA) to polyethersulfone (PES) substrates via self-initiated UV polymerization, followed by edge-tethering of GO to the PAA chains through amine coupling. The chemistry and interfacial properties of the unmodified PES, PAA-modified (PES-PAA), and GO-modified PES (PES-GO) substrates were demonstrated using ATR-FTIR, Raman spectroscopy, contact angle goniometry, and AFM to confirm the presence of PAA and covalently bonded GO on the substrates. Using SCFS, it was shown that peak adhesion force distributions for PES-PAA (with mean adhesion force $\bar{F}_{\text{Peak}}$ = -0.13 nN) and PES-GO ($\bar{F}_{\text{Peak}}$ = -0.11 nN) substrates were skewed towards weaker values compared to the PES control ($\bar{F}_{\text{Peak}}$ = -0.18 nN). The results show that weaker adhesion on PES-GO was due to a higher incidence of non-adhesive (repulsive) forces (45.9% compared to 22.2% over PES-PAA and 32.3% over PES), which result from steric repulsion allowed by the brush-like GO-PAA interface.

Table of Contents

Table of Figures

Table of Tables

No tables were included in this thesis.

Chapter 1: Introduction

As the global population of the world increases, the demand for fresh and potable water will continue to increase. As such, communities will be forced to find new and creative methods for maximizing the productivity of fresh water sources. Two areas of great opportunity for increasing/improving our water sources are desalinization and wastewater treatment/reuse. Membranes are a premier technology to address both these areas.

Membranes function by driving a pressurized feed solution through a selective semi-permeable structure via a pressure differential that preferentially rejects target constituents while allowing the permeation of water. Typically, membranes are operated in cross flow configuration where feed flow is tangential to the membrane surface (Fig. 1). This is done to prevent the accumulation of solute near the membrane surface which results in concentration polarization and decreased permeate quality.

Membranes are one of the most prevalent and dependable technologies for water treatment used worldwide [1]. They are heavily used in an array of sectors including, but not limited, to the treatment of ballast water [2], drinking water [3]–[6], wastewater [6], [7], the desalinization of sea and brackish groundwater[8], [9]. What makes membranes so effective is their unique ability to selectively filter out a variety of contaminants ranging from suspended particulates/colloids to small dissolved molecules and ions. The treatment and reuse of wastewater with membranes has become a primary focus in water conservation. One of the greatest potentials for membranes in the wastewater industry are membrane bioreactors (MBRs), which offer a very viable alternative to secondary clarifiers in wastewater due to their superior solid's retention, ease of operation, and small footprint

[10], [11]. In addition, membranes can be used as a polishing step on treated industrial effluent to produce reusable and even potable water [12].

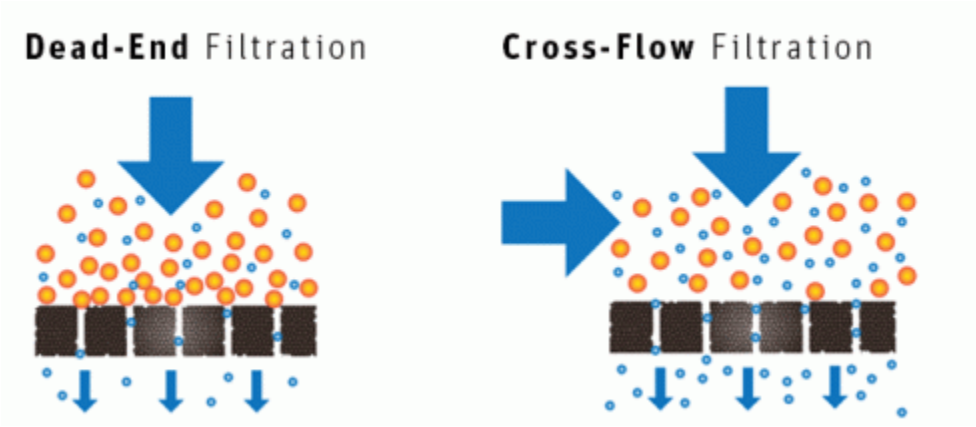

Figure 1 Schematic of membrane filtration for dead-end and cross-flow configuration.[1]

While membranes clearly offer a great deal of potential for water conservation they have one serious drawback; all membranes are inherently prone to fouling, particularly biological fouling [13]–[15]. Membrane biofouling occurs when bacteria and other microorganisms accumulate on the membrane surface and form biofilms, resulting in blocked pores/channels and an additional layer of resistance in which water must permeate through. Adverse effects of membrane biofouling include a reduction in permeate flux resulting in elevated operational pressure requirements and increased pumping costs, reduced membrane selectivity resulting in worsened solute rejection, accumulation of pathogenic colonies on the membrane surface, and biodegradation/deterioration of membranes [9]. Unlike other forms of fouling, biofouling is significantly harder to clean, often resulting in irreversible damage to membranes, permanent permeability loss, and shorter membrane life [16]. It is also much harder to prevent biofouling by pretreatment of

[1] Berghof Membranes. Accessed June, 2019. https://www.berghofmembranes.com/technology/

feed solutions with biocides; removing 99.99% of microorganisms from the feed can't guarantee mitigation of biofilms due to their ability to rapidly propagate across membrane surfaces. This is especially true for operations with high levels of nutrients in the feed streams such as wastewater treatment and desalination [16]. As such, a focal point of membrane research has been the development of anti-microbial surfaces. The most common approach has been the synthesis of biocidal coatings via the incorporation of nanomaterials that exhibit biocidal properties. Graphenic nanomaterials (GNMs, such as graphene, graphene oxide and carbon nanotubes) have risen to the forefront of this research due to their unique chemical properties, and biocidal nature. Graphene oxide nanosheets in particular have shown great promise given their superior anti-microbial properties [17]–[20].

The present work focuses on the application of graphene oxide (GO) nanosheets as anti-microbial additives to water filtration membranes. There has already been considerable research centered on incorporating GO into membranes to improve filtration properties and reducing biofouling [21]–[24]. However, recent studies have reported that GO functionalization of inorganic and polymeric substrates can actually increase their bio-adhesiveness.[25], [26]. The increased bio-adhesiveness observed from GO functionalization challenges the notion of GO films as anti-biofouling coatings. Meanwhile, the mechanism for bacterial adhesion to GO-functionalized interfaces remains poorly understood. A better understanding of the adhesive mechanism must be developed if graphene oxide is to be further realized as an anti-microbial surface. The focus of this paper is to modify the surface of water filtration membrane with GO nanosheets and use AFM-based single-cell force spectroscopy to directly measure the adhesive forces between

a model bacterium and membrane substrates with and without GO-modification. In addition, an array of characterization techniques will be used to demonstrate and explain the adhesive properties (or lack thereof) of GO and discuss the implications of these findings on the future of GO as an anti-microbial low-fouling surface for environmental applications.

Chapter 2: Literature Review

There are generally considered to be four types of fouling: colloidal/particulate fouling, organic fouling, inorganic fouling (scaling), and biological fouling (Fig. 2). The type of fouling that occurs on membranes is dependent on feed water conditions. Reverse osmosis (RO) membranes used for desalinization or brackish groundwater treatment often experience inorganic fouling due to the precipitation of salts on the membrane surfaces [27] while MF and UF membranes used in wastewater and drinking water treatment are more prone to colloidal or biological fouling [11]. However, due to the abundance of microorganisms and their ability to live in a wide variety of conditions, nearly all membrane operations are influenced by biofouling. The four types of membrane fouling are summarized below.

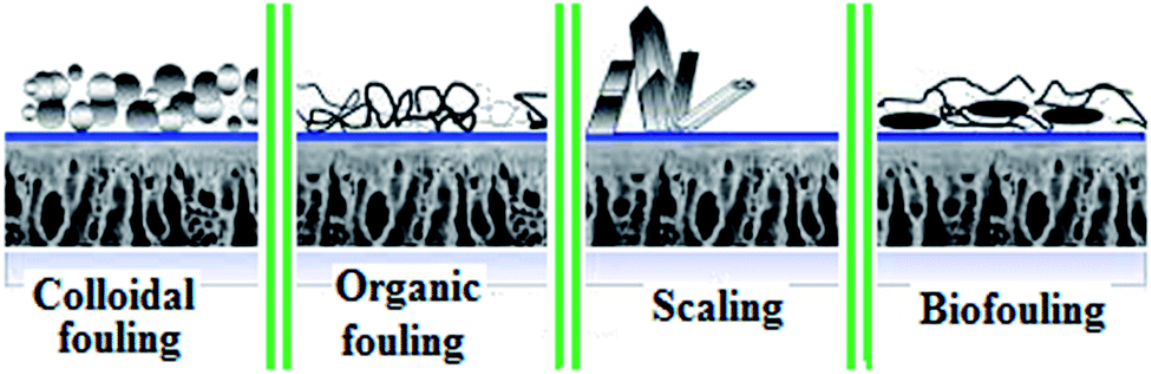

Figure 2 Schematic drawing showing the types of membrane fouling.[2]

Colloidal/particulate fouling

Colloids are suspended or dissolved particulates that range in scale from several micrometers down to nanometers. Typical colloids in aquatic environments are suspended

[2] A. Tiraferri, Membrane-based water treatment to increase water supply, Laboratory of Colloid and Surface Chemistry (LCSC) University of Geneva, http://www.colloid.ch/ membranes, accessed, June 2019.

inorganic particulates from aquifers such as silt or clay. Additional colloids found in water sources include very high molecular weight organic molecules such as polysaccharides, proteins and humic aggregates [28]. Colloidal fouling is most often associated with the partial or complete blocking of membrane pores, followed by the formation of cake on the membrane surface [29], [30]. As the membrane surface becomes caked, the pores become less water accessible leading to flux decline.

Organic fouling

Organic fouling of membranes is due to the presence of dissolved organic matter (DOM) in water. DOM is abundant in all surface water, most wastewaters, and sewage [31]. Types of DOM include synthetic organic compounds (SOCs, such as flocculating agents, soaps, and dies), disinfection byproducts (DBPs, such as trihalomethanes, halogenic acetic acids, and chlorine hydrates), and natural organic matter (NOM) [28]. NOM is formed by the decay of plant and animal matter in the environment and is prevalent in most drinking water sources [32][28]. Depending on the type of DOM present, organic fouling can occur by adsorption into the membrane pores resulting in partial or complete obstruction to water flow, formation of gel layer across the membrane surface concealing the pores, and/or the tethering of particulate matter across the membrane resulting in decreased permeability [28].

Inorganic fouling

Inorganic fouling (often referred to as scaling) is caused by the precipitation of inorganic compounds resulting from oxidation and hydrolysis during membrane filtration. Crystallization is the primary form of inorganic fouling. Typically, in water filtration operations involving the use of RO, salt ions are rejected and concentrated in the reject

stream up to 10 times their feed concentrations [28]. Dissolved compounds exceed their solubility limit resulting in the precipitation/crystallization of salts onto the membrane surface. One common inorganic foulant with low solubility is $CaCO_3$ which is used extensively in lime softening for drinking water treatment. Alternatively, suspended inorganic particulates can be deposited onto membranes via advective transport. Once lodged, these particulates act as nucleation sites for additional scaling of the membrane [28]. Most inorganic fouling occurs in operations dealing with high dissolved solids. Operations could include the desalinization of salt water, the treatment of brackish groundwater, and the reuse of industrial wastewater [27], [33].

Biofouling

Biofouling of membranes involves the growth of biofilms across the membrane surfaces. In addition to clogging channels of porous membranes, these biofilms coat the membrane surface, reducing membrane selectivity and acting as an additional layer for water permeation [34]. Biofilm formation is a complex process that can be affected by a wide range of factors including the microbe species, membrane surface chemical composition, membrane surface roughness, feed water compositions, and even the fluid mechanics to and through the membranes[14], [35], [36]. In general, biofilm formation can be broken down into several different phases: transport/deposition of cells to a surface, adhesion onto the surface, and biofilm growth/propagation, and finally dispersion. Fig. 3 shows a representative schematic of this process with the attachment phase encompassing both bacterial deposition and adhesion.

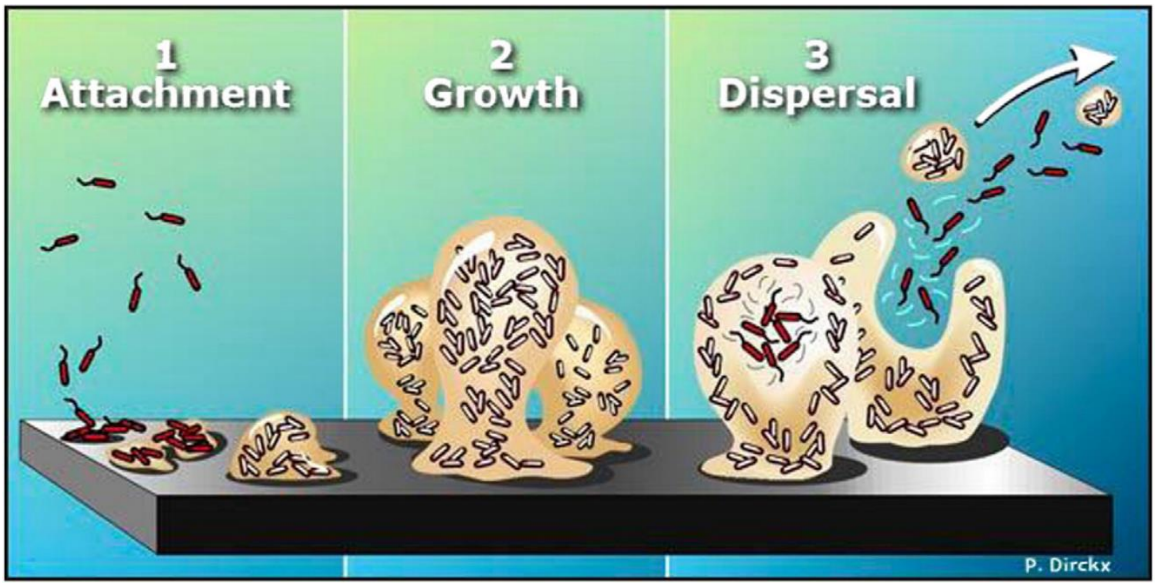

Figure 3 Sequence of events leading to the formation of a Biofilm.[3] [8]

Mechanism of Biofouling

Deposition

In the first phase of biofilm development, microbial cells are transported to the surface of the membranes. As microbes approach the surface they must overcome an energy barrier resulting from attractive and repulsive forces prior to establishing direct contact. These forces can consist of Van der Waals interactions, electrostatic repulsive forces and acid base forces [13]. Membranes are predominantly negatively charged on their active surface to promote water transport via attraction to hydrophilic functional groups such as carboxylic acid [37], while microbes' membrane contain negative charged groups hydrophilic head groups. As such, electrostatic repulsive forces between the bacteria and membrane surface play a significant role in deposition. Feed water ionic strength and pH also influence deposition. When the pH is neutral or even slightly acidic, the carboxylic

[3] . The Biofilms Hypertextbook: Introduction to Biofilms Alfred B. Cunningham, John E. Lennox, and Rockford J. Ross, Eds. 2001–2008. Accessed June 2019.

groups on the microbe and membrane surfaces will shift to their protonated neutral state [38]. Once neutral, the repulsive energy from their like charges is greatly reduced, making deposition much more favorable. In addition, increased ionic strength influences the Debye length, thus affecting the range of electrostatic interactions between cells and surfaces [13].

Adhesion

Once microbes overcome the energy barrier necessary to deposit onto the membrane surface, they must irreversibly adhere to the surface. Adhesion is general believed to be the most critical step in establishing biofilms on membrane surfaces and is also the least understood [13], [39], [40]. The adhesive interactions between cells and membranes have been shown to be dependent on many chemical and physical factors including the microbe type, the composition of EPS secreted, surface charge, and surface roughness [34]. In particular, membrane hydrophobicity plays a significant role in adhesion [13], [41]. More hydrophobic, non-polar surfaces have been shown to increase biofouling [16]. The opposite is the case for hydrophilic membranes. This can be explained by considering the packing of water molecules near the membrane surface. Membranes with higher hydrophilicity have a greater affinity for water molecules. To minimize the interfacial energy at the membrane-water interface, water molecules will pack more closely at the surface. For cells to adhere to the membranes, they must first penetrate through this packed water layer which is less thermodynamically favorable when compared to hydrophobic membranes. It is believed that the physical appendages of bacterial cells (flagella, fimbriae and pili) are used to overcome the repulsive energy associated with this packed water layer and electrical double layer at the membrane surface (due to charged surfaces) to establish irreversible adhesion [40], [41]. In addition, cells excrete EPS (Extracellular polymeric substances) that

produce a hydrophobic conditioning film on surfaces. This hydrophobic coating is used as a mechanism to promotes cellular adhesion by altering characteristics of the surface such as charge, hydrophobicity, and roughness [42].

Propagation

Once microbes have irreversibly adhered to the membrane surface, they begin the growth phase in biofilm development. In this phase, secretion of EPS (naturally produced high molecular weight biopolymers, such as proteins, polysaccharides, and lipids) is increased and the EPS matrix is formed. This matrix binds the microbes together in microbial aggregates and establishes the functional and structural integrity of biofilms [8]. In addition, the EPS matrix is largely considered the most influential component determining the physiochemical properties of biofilms [34] and is typically the largest fraction (50-80%) of the total organic matter in biofilms [8], [28]. Main advantages of microbes within the matrix are increased colony stability, protection from harsh environmental conditions, sequestration of nutrients, and the development of synergistic relationships with other species [8], [43]. The additional protection is exhibited in a shielding effect in which the EPS molecules and exterior cells shelter the interior organisms from potential harsh conditions in the water (pH, biocides, etc.) by limiting mass transfer through the EPS matrix, thus increasing the resilience of the microbial community [8], [43]. Furthermore, microbes of possessing diverse metabolic pathways are aggregated in close proximity within the matrix, promoting sequential degradation of substances that were otherwise not biodegradable by a single species (cometabolism) [8], [43]. Often this syntrophic effect is exhibited in stratified layers of the biofilm. In total, the syntrophic interactions possible within the shielded EPS matrix results in rapid biofilm growth and resilience.

Dispersion

The final stage of biofilm formation is dispersion. In this stage, sections of the biofilm slough off resulting in resuspension of viable bacteria. These cells then deposit and adhere to other locations, repeating the process of biofilm formation and further propagating the biofilm across the membrane surface [8].

Impact of Biofilms

Almost all membrane applications are hampered by biofouling in some form or another. Arguably one of the most substantial influences of biofouling has been on the practicality of membrane bioreactors (MBRs) in wastewater treatment. As previously mentioned, MBRs use low pressure membranes (UF and MF) as a substitute for traditional secondary clarifiers as a means of retaining biomass in activated sludge reactors. Membrane bioreactors rely on size exclusion rather than gravity to achieve physical separation of wastewater from biomass and are able to achieve 100 percent retention of biomass at any sludge retention time [28]. While the pressure requirements are not inconsiderable, the reduced footprint and increased operational control achieved by MBRs makes them incredibly promising for wastewater treatment and water reuse [44]. Unfortunately, membranes used in MBRs are incredibly prone to biofouling due to the inherent nutrient richness and biological density of microorganisms in activated sludge basins [11]. In order for membrane technologies such as MBRs to truly thrive, researchers must find ways to mitigate biofouling.

Biocidal Membrane Modifications

There has been significant research into modification of membranes to reduce their propensity to biofoul. Much of this research is focused on incorporating biocidal-exhibiting

nanomaterials into membrane structures and surfaces. This includes, but is certainly not limited to, silver nanoparticles (Ag NP) [45], [46], Zinc oxide (ZnO) [47], copper [48], silica (SiO_2) [49] , and carbon nanomaterials such as graphene, graphene oxide (GO) and carbon nanotubes (CNTs) [21], [50]–[52]. Unfortunately, many metal nanoparticles tend to dissolve or leach off the membrane leading to decreased biocidal capacity of the membrane in addition to environmental contamination. An example of this is membranes functionalized with silver nanoparticles. These membranes are prone to secreting dissolved silver ions during operation, resulting in a decrease in biocidal capacity overtime and an increase in biofouling propensity [45],[53]. While it has been shown that silver NP coatings can be regenerated, the temporary reduction in bacterial inactivation and the environmental impacts associated with the leached particles can't be avoided [46]. As such, non-leaching, non-depleting biocidal coatings offer significantly more potential for biofouling mitigation.

Graphemic nanomaterials (GNMs) possess the most potential for biocidal coatings owed to their ability to functionalized with membranes in a permanent non-leaching fashion. Furthermore, the biocidal mechanism for bacterial inactivation of GNMs is based on cellular contact and is not subjected to regeneration requirements [54]. Graphene oxide (GO) in particular has shown considerable capacity as an anti-microbial surface owing to its high specific surface area (~2,630 $m^2 g^{-1}$)[55], single-atom-thickness (0.34nm), superior hydrophilicity, and strong biocidal properties [46], [52], [56]. They offer considerable promise as membrane materials [57]–[59] and adsorbents for the removal of water contaminants [60]. Currently, graphene oxide nanosheets are the most common GNM used in the development of polymeric hybrid membranes for water treatment [61].

Graphene Oxide

Graphene oxide is synthesized from graphene nanosheets, one-atom-thick 2D sheets of sp^2 hybridized carbon atoms closely packed in a hexagonal lattice. GO nanosheets can be synthesized in a variety of manners including the Hummers, Brodie, or Staudenmaier methods [61]. Typical synthesis involves the oxidative treatment of graphene to graphene oxide which creates hydrophilic hydroxyl, carboxyl, and epoxide groups concentrated on the edges and surface.

Incorporation of Graphene Oxide into Membranes

One feature that makes graphene oxide so promising as a anti-microbial surface is its ability to be incorporated into membranes. There are four general methods in which membranes have been reported to have been functionalized with graphene oxide: i) casting, ii) interfacial polymerization, iii) layer-by-layer assembly, and iv) surface modification [61].

Casting

Casting is one of the most common ways of fabricating porous MF and UF membranes and porous support layers for thin film composite (TFC) membranes [61]. Functionalization with GO is typically performed by dispersion of graphene oxide nanoparticles into the casting solution. The solution is then spread at a uniform thickness over a flat surface using a casting knife and submerged into a solvent bath, often deionized water, where the dissolved polymer precipitates via phase inversion forming the GO-membrane composite. There have been numerous functionalized graphene oxide-incorporated membranes prepared by phase inversion over a variety of polymer matrices including polysulfone (PSf) [62], poly(vinylidene fluoride) (PVDF) [63], and poly(vinyl chloride) (PVC) [64] to name a few. One issue associated with this functionalization method is that much the

homogenously incorporated GO particles are contained within the membrane bulk, resulting in less efficient use of the GO compared to surface modification techniques.

Interfacial polymerization

Interfacial polymerization has been effective mechanism for forming the active layer of membranes. These active layers are responsible for salt rejection and directly affect water permeability [65]. Graphene oxide-incorporated TFC membranes have showed significant promise in NF, RO, and FO membranes [61]. A typical approach for interfacial polymerization is to disperse graphene oxide into an aqueous phase of m-phenylenediamine (MPD) and deposit onto a support layer such as polysulfone or polyethersulfone (PES). Trimesoyl chlorine (TMC) dissolved in n-hexane is then deposited onto top of the aqueous MPD initiating interfacial polymerization. The result is a homogenously distrusted graphene oxide-incorporated polyamide active layer on top of the polymer support [61]. In most cases, the GO functionalized membranes showed increased hydrophilicity and negative charges at the surface which resulted in improvements in the operational capabilities of the membranes. Additionally, interfacial polymerization utilizes the graphene oxide only in the polyamide active layer and not support layer, resulting in reduced quantity of nanoparticle relative to the previously mentioned casting method.

Layer-by-layer (LBL) assembly

Layer-by-layer assembly requires multiple layers of graphene oxide nanosheets to be constructed on the membrane surface. Each layer can be adhered through a variety of forces. Successful LBL assembly has been performed using covalent bonds, hydrogen bonding, electrostatic interactions, and van der Waals forces [61], [66]. Advantages to this

method are that all GO is concentrated at the surfaces, maximizing the particle use efficiency.

Surface Modification

Surface modification, like the LBL method, involves the binding of graphene oxide onto the membrane surface, with the exception that only one layer is formed. This can generally be achieved in two ways: i) covalent bonds induced by cross-linking/surface grafting and ii) noncovalent bonding via coating or filtration [61]. The advantage to the first approach is the strong attachment of graphene oxide distributed relatively evenly across the membrane surface, which improves the lasting durability and efficacy of the membrane coating. Successful functionalization of graphene oxide has been achieved across all membrane types (i.e. MF, UF, NF, RO etc) via this method [61]. Several studies have been published in which reactive amino-esters (EDC/NHS) were used in tandem with ethylenediamine (ED) to crosslink graphene oxide uniformly across the polyamide layer of TFC membranes [52],[46]. The modified membranes were shown to exhibit significant biocidal properties in regards to E. *coli* [52].

The second approach utilizes non-covalent bonds (i.e. hydrogen bonding and van der Waals interactions) to secure graphene oxide to the membrane surfaces. This method is typically performed via coating or filtration processes with additional supplied pressure is applied to force contact graphene oxide with the membrane surface. Successful functionalization via non-covalent interactions has been reported across an array of membrane materials [61]. While this method tends to be easier, the long-term functionality of the membrane coatings is often reduced due to hydrodynamic shearing of the weaker

noncovalent bonds tethering GO to the membrane. As such, a covalently bonded procedure is preferred.

Biocidal Properties of Graphene Oxide

As previously laid out, graphene oxide can be incorporated into membranes in a variety of manners, with the preferred method covalently tethering GO to the membrane surfaces. This is done to maximize the available GO at the membrane surface, thus increasing the bacteria-graphene interaction and bolstering the biocidal potential of the coating. Unlike other biocidal coatings, graphene oxide has been shown to exhibit biocidal characteristics when contacted directly with bacterial cells [46], [52], [56]. Bacterial inactivation has been reported to exceed 80%, significantly better than other GNMs [46]. Several mechanisms for bacterial interaction have been stated upon contact including physical disruption of the cell wall [67], and charge transfer and generation of reactive oxygen species [67], [68], [69]. These properties are similar amongst most graphemic nanomaterials. However, a biocidal mechanism unique to graphene oxide is the knife-like action of GO sheets. It has been shown that graphene oxide sheets oriented orthogonal to surfaces are able to cut into cell membranes and extract large amounts of phospholipids, resulting in cell death [70]. This additional biocidal mechanism make GO a very potent option for anti-microbial surfaces. While the biocidal mechanisms for GO are increasingly well understood, there is less information available regarding the bioadhesion mechanisms on the graphene oxide interface. One such method that can be used to elucidate these mechanisms is AFM-based single-cell force spectroscopy.

Single Cell Force Spectroscopy

To understand this technology better, the principles of atomic force microscopy (AFM) are first explained. Atomic force microscopy involves the use of a laser-calibrated cantilever to measure microscopic forces between two materials. Measurements are performed by extending and retracting a substrate-coated cantilever against a surface of interest. The laser deflection upon extension and retraction of the cantilever is then used to determine the compressive and retractive forces and their ranges of interaction between the substrates. Recent advancements in AFM-based single-cell force spectroscopy (SCFS) allow us to examine the nanoscale interactions of bacterial adhesion onto surfaces. SCFS works by immobilizing a single cell onto a cantilever tip which is subsequently contacted with the substrate of interest in an identical manner as AFM to measure the repulsive and adhesive forces (Fig. 4). Analysis of the retraction curves (adhesive forces) allows the elucidation of the extracellular biomolecules involved in the bioadhesion process.

While graphene oxide has been shown to exhibit a wide range of biocidal properties, further development of graphene oxide coated membranes has been hindered by an undeveloped understanding of the bioadhesive mechanisms between bacterial cells and graphene oxide sheets. Studies have attempted to analyze these adhesive forces with inconsistent results. A study performed by Tu et al., suggested GO sheets pierce bacterial cell membranes in an orthogonal manner while other studies have shown predominantly repulsive interactions between GO-coated AFM probes and the negatively charged cell membranes of E. *coli* bacteria [70]. It has more recently been shown that the spatial orientation of graphene oxide bound to silicon surfaces plays a significant role in the adhesive forces exhibited between GO sheets and bacterial cells, showing that GO sheets oriented flatter across a surfaces

tend towards higher adhesion forces [25]. These contradictory results further cloud whether the hydrophilic graphene oxide coatings would reduce or increase the propensity for membrane biofouling.

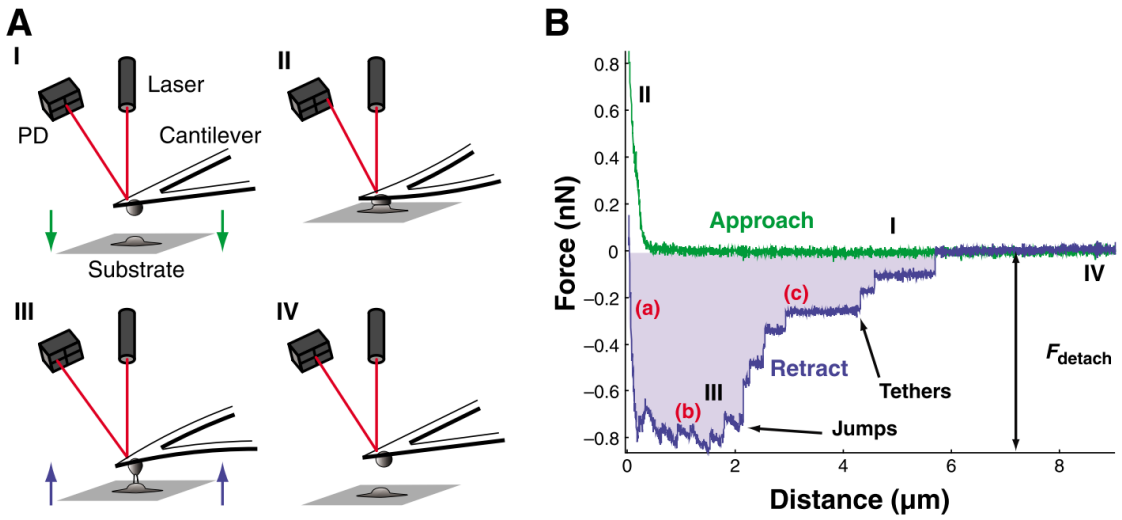

Figure 4. Schematic diagram of AFM-based single-cell force spectroscopy
Shows the (A) experimental setup and (B) representative force curves for SCFS [71].

A recent study using SCFS have compared the bacterial adhesion pristine and modified membranes with hydrophilic coatings and found that the hydrophilic coatings tended to decrease mean adhesion forces. However, the same study found that increased bacteria-membrane contact time revealed similar adhesion across all membranes, indicating that hydrophilicity is likely not enough to determine the antifouling capabilities of membranes [39]. The goal of this research is to apply this same methodology to graphene oxide-functionalized membranes. Given the unique and promising biocidal properties of GO, it is very much worth investigating the adhesive (or antiadhesive) nature of GO on a membrane. Analysis of commercial membranes functionalized with graphene oxide with

SCFS should yield valuable insight into whether the biocidal and physical properties of GO promote membrane biofouling.

Chapter 3: Do Graphene Oxide Nanostructured Coatings Mitigate Bacterial Adhesion?

Given graphene oxides' robust biocidal properties, there is significant promise for GO as a building block for anti-microbial surfaces, However, the extent to which GO mitigates bacterial adhesion, the most critical step in biofilm formation, is still uncertain. The purpose of this research was to use AFM-based single-cell force spectroscopy to demonstrate that GO nanosheet coatings bound to a membrane surfaces by a hydrophilic polymer brush layer reduces the adhesion of *Pseudomonas fluorescens* cells, while preserving GO's intrinsic biocidal activity. This research is laid out as follows: first successful tethering of graphene oxide sheets to a polyethersulfone (PES) membranes by poly(acrylic acid) chains via a novel functionalization technique is demonstrated. Then, it is shown that the biocidal properties of GO sheets are maintained on the membrane surface. Finally, SCFS is utilized in addition to several other membrane characterization techniques to demonstrate and explain the adhesive properties of GO and discuss the implications of these findings on the future of GO as an anti-microbial low-fouling surface for environmental applications.

Materials and Methods

Graphene Oxide Functionalization

Substrates

All coatings investigated were formed on polyethersulfone (PES) substrates. Commercially available PES ultrafiltration (UF) membranes were used (30 kDa molecular weight cutoff; Synder Filtration, Vacaville, USA). PES membranes were soaked in 50% glycerin solution and stored at 4 °C. Prior to use, the membrane substrates were rinsed with ultrapure (UP)

water (18.2 MΩ cm, Barnstead, Thermo Fisher), soaked in 25 vol.% aqueous isopropanol for 24 hours, and thoroughly rinsed again with UP water to remove any residual preservatives.

Poly(acrylic acid) Grafting

Self-initiated UV graft polymerization was used to grow poly(acrylic acid) (PAA) on PES [37], [51], [72]–[74]. PAA chains were subsequently used to functionalize substrates with GO. A schematic diagram of the surface modification protocol is shown in Fig. 1. An aqueous acrylic acid (AA) solution (10 vol.-%) was prepared from a 99% AA stock solution (Sigma Aldrich) with UP water. PES coupons (9×14 cm^2) were attached to PTFE frames with a holding volume of 112 mL. The PES substrates and the AA solution were brought to a glove box, from which oxygen had been purged to a concentration < 500 ppm to prevent premature radical termination. The solution and the substrates were left to equilibrate with the atmosphere inside the glove box for 15 minutes to lower the dissolved oxygen concentration in the AA monomer solution. Next, 10 vol.-% AA solution was poured over the PES (affixed to the PTFE frame) and allowed to soak the PES substrate. After 15 minutes, excess AA solution was removed, leaving a thin liquid film of AA monomer solution on the surface (Fig. 5 (a)). By casting the monomer solution as a thin film, the UV penetration depth was increased, thus accelerating the polymerization kinetics on the substrate. Subsequently, the AA-soaked PES surface was irradiated with a UV lamp (Spectroline Model EF-160C) positioned ~2 cm above the substrate. Irradiation was carried out for time periods ranging from 10 to 60 seconds. After irradiation, the substrates were rinsed thoroughly and soaked in UP water for 24 hours to remove unreacted monomers.

This step resulted in PAA-functionalized PES substrates (Fig. 5 (b)), which is referred to as PES-PAA for the remainder of the paper.

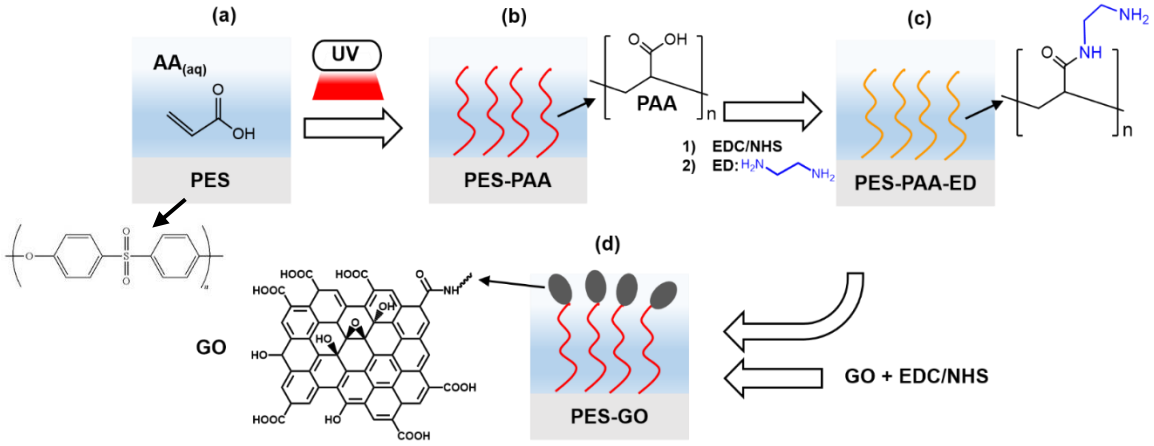

Figure 5. Schematic of polyethersulfone (PES) surface modification with (GO).

Self-initiated UV polymerization (a-b) results in growth of poly(acrylic acid) (PAA) chains from acrylic acid (AA) monomers in aqueous solution, yielding PES-PAA substrates. (c) EDC/NHS-mediated amine coupling binds ethylenediamine (ED) linkers to the PAA chains, resulting in PES-PAA-ED substrates. (d) EDC/NHS-activated GO nanosheets react with primary amines in the ED linker to covalently tether GO to the substrates (yielding PES-GO substrates).

Substrate Functionalization with GO

Single-layer graphene oxide (GO) was purchased from Cheap Tubes (Grafton, VT, USA). Characterization by AC mode AFM was carried out to reveal an average nanosheet thickness of 0.8 ± 0.1 nm, consistent with single sheets [25]. In addition, sub-micron lateral dimensions (Appendix A, Fig. S1 (a) and (b)) was in agreement with the manufacturer's specifications (i.e., 300-800 nm). A negative zeta potential was observed for GO in aqueous dispersion (Appendix A, Fig. S1 (c)), indicative of deprotonation of carboxylic acid groups in the nanosheet edges [75]. The oxygen content of GO was 35-45%, per the manufacturer's specifications. The Raman spectrum of GO nanosheets deposited on a

silicon wafer (Appendix A, Fig. S1 (d)) exhibited the D (~1350 cm^{-1}) and G (~1590 cm^{-1}) bands characteristic of GO [76]. Substrates were functionalized with 250 μg mL^{-1} GO dispersions prepared from 2 mg mL^{-1} stock dispersions. GO suspensions were made colloidally stable through bath sonication for 24 hours. PES-PAA substrates were functionalized with GO by adapting the procedure developed by Perreault et al.,[52] which was based on amine coupling [77]. Carboxylic acid functional groups in the grafted PAA chains were activated to amine-reactive esters with 4 mM 1-ethyl-3-(3-dimethylaminopropyl)carbodiimide hydrochloride (EDC, 98%, Sigma) and 10 mM *N*-hydroxysuccinimide (NHS, 98%, Sigma). Solutions were buffered at pH 5 with 10 mM MES (BioXtra, Sigma) supplemented with 0.5 M NaCl. The EDC-NHS activation step was carried out for 60 minutes under ambient conditions on a benchtop shaker at 30 rpm. Substrates were then rinsed gently with UP water. The amine reactive esters on the PES-PAA surface were then contacted with 10 mM ethylenediamine solution (ED, BioXtra, Sigma) buffered at pH 7.5 by 10 mM HEPES (99.5%, Sigma) with 0.15 mM NaCl. The ED amine coupling step was performed for 30 minutes. The result was PES-PAA-ED substrates, as shown schematically in Fig. 5(c). Next, the carboxylic acid functional groups along the GO nanosheet edges were reacted to amine reactive esters in a similar way. A GO dispersion (10 parts, 250 μg mL^{-1}) was mixed with 2 parts 100 mM MES buffer, followed by 1.75 parts 20 mM EDC in 10 mM MES buffer, and 1.75 parts 50 mM NHS in 10 mM MES buffer. The pH of the solution was then lowered to 5.5 by addition of 1 M HCl dropwise (to minimize flocculation of GO nanosheets) and allowed to react for 15 minutes. Subsequently, the pH was raised to 7.2 by addition of 1 M NaOH dropwise. The GO dispersion was then poured over the ED-functionalized surface (PES-PAA-ED),

covered, and allowed to react for 1 hour on a benchtop shaker at 30 rpm. Reaction between the amine-reactive esters in GO and the primary amine groups on the surface of the ED-modified membranes resulted in covalent linkage of the GO nanosheets to produce PES-GO membrane (Fig. 5(d)). Finally, PES-GO samples were thoroughly rinsed and sonicated for 5 minutes to remove non-covalently bonded GO. All substrate samples were stored in ultrapure water at 4 °C until use.

Statistical Analysis

Unless stated otherwise, two-sided unpaired *t*-tests, presuming unknown but equal population variances, were used to determine the statistical significance of the results.

Membrane Characterization Techniques

Several techniques were used to characterize the unmodified and modified membranes. Each of the techniques, including the instruments and their respective procedures, are discussed in detail below.

Fourier-Transform Infrared Spectroscopy (FTIR)

Attenuated total reflectance (ATR) FTIR was utilized to characterize the functional groups covering the membrane surfaces throughout the modification procedure. Membrane samples were dried overnight in a desiccator to remove any residual water that might appear on the FTIR spectra. Spectra of desiccator-dried specimens of each substrate type were acquired in an FTIR spectrometer (Nicolet Series II Magna-IR System 750) equipped with an ATR cell. The spectra were collected in terms of % reflectance at a resolution of 0.241 cm^{-1}.

Raman Spectroscopy

Raman spectroscopy was used to characterize GO functional groups across the membranes. Membrane samples were tested by first drying them overnight in a desiccator. Raman spectra were obtained with an Alpha300R Raman microscope (Witec). For each membrane specimen, 20 × 20 μm^2 Raman scans were acquired at a 0.5 μm resolution, on randomly chosen sections of the substrates. At each point in the 2D scan, the ratio of the area under the D band of GO (observed at 1350 cm^{-1}) [76] and the area under a prominent PES peak (observed at 1146 cm^{-1}) was computed to generate maps characterizing the spatial distribution of GO nanosheets. In addition, a mean Raman spectrum was generated by averaging the spectra collected at each point on the 2D scan.

Contact Angle

Membrane hydrophobicity was characterized by oil-in-water contact angle measurements via the captive bubble method. The contact angle between submerged droplets of n-decane and the membrane were measured in an aqueous environment using a goniometer (Ramé-Hart, Model 200) and DROP Image software (Ramé-Hart). Membrane substrates were affixed to a surface with the functionalized side facing a liquid cell containing ultrapure water. The membranes were then submerged in ultrapure water. A J-shaped needle was used to inject n-decane droplets (~10μL) onto the membrane surface. The droplet sizes were kept at this volume for each measurement to reduce the skewing effect on the contact angle by increased buoyant forces of larger bubbles. For each substrate type, at least 14 contact angles were measured across three independently functionalized membranes.

Surface Charge

Membrane surface charge was characterized by zeta potential. Streaming potentials of the membrane surface were measured using a SurPASS electrokinetic analyzer (Anton-Paar) from a pH of 10 to a pH pf 4 in 1 mM KCl solution. Varying aliquots of 0.05mM HCl were used to lower the pH. An adjustable gap cell with a fixed distance of 120μm was used. Three separately functionalized specimens were characterized for each membrane type. The zeta potential was then determined from the streaming potential data using the Smoluchowski-Helmholtz equation [78].

Nanoscale Roughness

Nanoscale roughness of the membrane surfaces was characterized using atomic force microscopy (AFM). Measurements were performed with an MFP-3D-Bio AFM (Asylum Research) equipped with a liquid cell. AC mode AFM scans (5×5 μm^2, scan rate = 0.25 Hz) of two specimens of each substrate type were obtained in phosphate-buffered saline (PBS) at pH 7.4 using a silicon nitride cantilever (SNL probe "C", nominal $k = 0.24$ N m^{-1}, Bruker). The surface topography was quantified in terms of the root-mean-squared roughness (R_{RMS}) determined in 1×1 μm^2 areas of each of the AFM scans for a total of 8 roughness calculations for each substrate type.

Biocidal Plate Assay

The biocidal activity of the substrate interfaces was characterized by colony counting [52]. *Pseudomonas fluorescens*, a Gram-negative, biofilm-forming bacterium was used as a model organism [39]. *Pseudomonas fluorescens* ATCC 13525 bacteria were prepared in an overnight culture in 50mL of autoclaved LB broth under constant 125rpm stirring at 30^{o}C in an incubator. Bacterial suspensions were diluted 1:25 in autoclaved LB broth at

30°C. Stirring was increased to 175rpm for approximately three hours. Bacterial dilutions were harvested in the mid-exponential phase (OD ≈ 0.6), centrifuged three times at 5,000G for 1 minute, removing the supernatant and re-suspending the pellet with 1mL PBS (pH 7.4) each time. After the final re-suspension, the 1mL bacterial suspension was diluted to 10mL with fresh PBS and 1-cm^2 membrane coupons were immersed in 1mL of bacterial suspension for 1 hour. Membranes were then removed, gently rinsed with PBS, and placed in 10mL of fresh PBS in 50mL falcon tubes, where they were bath sonicated for 10 minutes. The resulting solutions were then diluted 1:100 and 50uL aliquots of each dilution were smeared over agar plates evenly with a sterilized glass rod. The plates were then incubated overnight at 30°C and the colonies were counted after 24hrs. The experiment was repeated two additional times for a total of three replicates for each membrane substrate.

Single Cell Force spectroscopy (SCFS)

The adhesion of *P. fluorescens* cells to the surface of control and functionalized substrates was quantitatively investigated using single-cell force spectroscopy (SCFS). Bacterial cells were grown and cultivated following the same protocol of the biocidal assay. The experimental procedure of SCFS was followed from an earlier study performed in the same lab and detailed in a recent publication [39]. An individual *P. fluorescens* cell was adhered to a tip-less AFM cantilever (MLCT-O10 probe "C", nominal k = 0.01 N m^{-1}, Bruker) on which a polydopamine wet adhesive layer had been deposited from a dopamine hydrochloride solution (4 mg of dopamine hydrochloride per milliliter of Trizma buffer, pH 8.5) shortly before adhering the cell. An MFP-3D-Bio AFM (Asylum Research) integrated to a Zeiss Axio Observer A1 inverted optical microscope was used to perform bacterial cell adhesion force measurements. All forces were determined at room

temperature (25 °C) in a liquid cell filled with PBS solution at a pH 7.4. Force curves, comprising extension-retraction cycles, were carried out at a cantilever speed of 400 nm/s, a piezo dynamic range of at least 3 μm, a trigger force (the maximum force applied to the cell as it contacts the substrate) of 600 pN. A dwell time (the time in which the bacteria is contacted upon reaching the trigger force) of 0 s was used. For each substrate type, a total of ≥ 98 force curves were collected with at least 2 independently cultivated bacterial cells, on ≥ 2 different substrate specimens of each type. Force curves were acquired at randomly chosen sites on the substrate. At each randomly chosen location, up to three force curves were collected to minimize deposition of extracellular polymeric substances (EPS) on the substrate. After each experiment, the cell viability was determined using a live/dead assay (BacLight, Thermofisher). Only data collected with a live cell that remained at its initial location were reported.

Characterization Results

The previously mentioned techniques were used to characterize the membranes throughout the membrane modification procedure and to verify the efficacy of the modifications.

Surface Chemistry

Fourier-Transform Infrared Spectroscopy (FTIR)

FTIR spectroscopy was used to assess the efficacy of PAA grafting by examining the prominent IR bands present in the AA monomer. AA polymerizes on the PES substrate due to UV-generated free radicals formed on the PES surface, which react with the vinyl double bond of the AA molecule, leading to the formation of PAA chains covalently bonded to the substrate [74]. The degree of grafting (i.e., the extent of AA polymerization on the PES substrate), and the kinetics of polymerization, are influenced by the UV irradiation time and UV wavelength [74], [79]. PES substrates soaked with a thin liquid film of 10 vol.-% AA solution were exposed to UV light for 10-60 seconds. The FTIR results for the PES control and PES-PAA substrates are shown in Fig. 6. The peak visible at 1580 cm^{-1}, observed in all samples, was due to vibration of the aromatic rings in PES [80]. In addition, IR bands were seen which corresponded to carboxylic acid groups in PAA, namely a peak at 1700-1730 cm^{-1} due to C=O stretching vibration [81], and multiple bands in the 2500-3300 cm^{-1} range due to COO-H stretching [81]. These peaks increased monotonically with irradiation time, in line with increasing degree of PAA grafting [79]. The remainder of the study was focused on PES substrates fabricated with a 10-s UV irradiation step, which resulted in materials with nanofiltration-like water permeability coefficient and divalent ion rejection (see Appendix A for methods and results). Irradiation times > 10 s resulted in a dense PAA layer and a steep loss in water permeability.

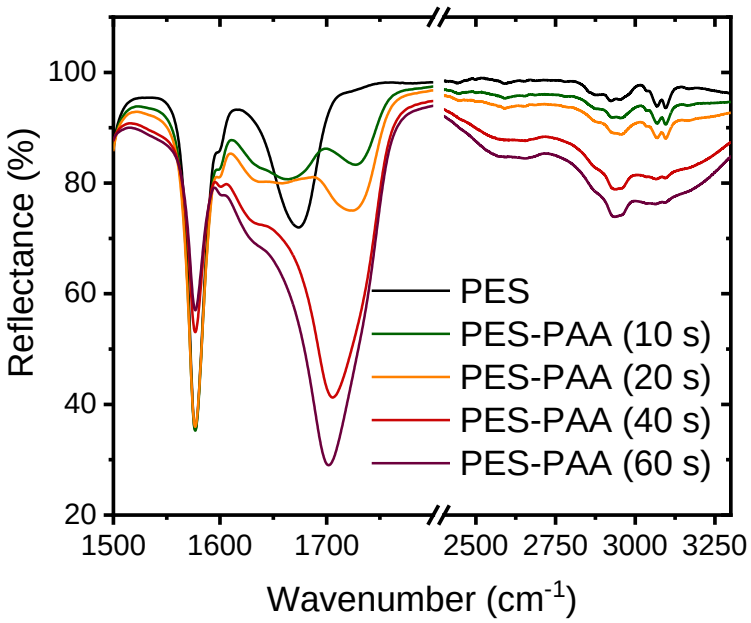

Figure 6. FTIR spectra of PES and poly(acrylic acid) (PAA)-functionalized PES. (PES-PAA, prepared with different UV irradiation times noted in the figure).

The FTIR spectra of the PES, PES-PAA (10-s UV irradiation) and PES-GO substrates are presented in Fig. 7. The spectrum corresponding to PES-GO shows an increase in the COO-H stretching band at 3300 cm^{-1} relative to PES-PAA, which was attributed to carboxylic acid functional groups present in the GO nanosheet edges [75]. In addition, PES-GO substrates exhibit a peak at ~2900 cm^{-1} which was absent in the other substrates. This peak was likely an N-H stretching vibration band (typically observed at 3100-3500 cm^{-1} [81]) due to primary amines that remain unreacted after the GO modification step.

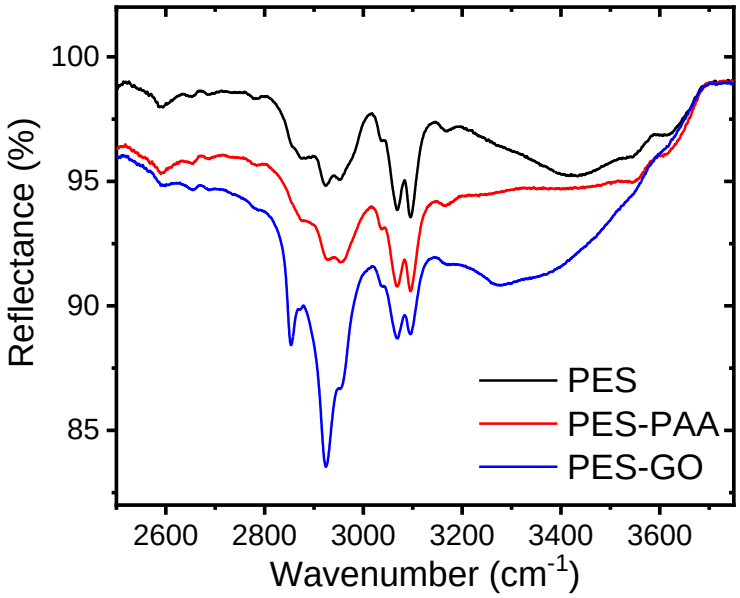

Figure 7. FTIR spectra of control PES, PES-PAA, and PES-GO.

Spectrums of pristine PES, poly(acrylic acid) (PAA)-functionalized PES (PES-PAA, 10-s UV irradiation), and GO-functionalized (PES-GO) substrates.

Raman Spectroscopy

The presence of graphene oxide on the PES-GO substrates was confirmed using Raman spectroscopy. The average of 1600 spectra scanned over a 20 × 20 μm^2 area of each specimen is presented in Fig. 8. The PES-GO substrate prominently shows the G and D bands of graphene oxide [76], thus confirming functionalization of PES with GO. All substrates show similar chemical signatures due to polyethersulfone, e.g., peaks at 790, 1070, 1107, 1146, 1580 and 1601 cm^{-1} [82].

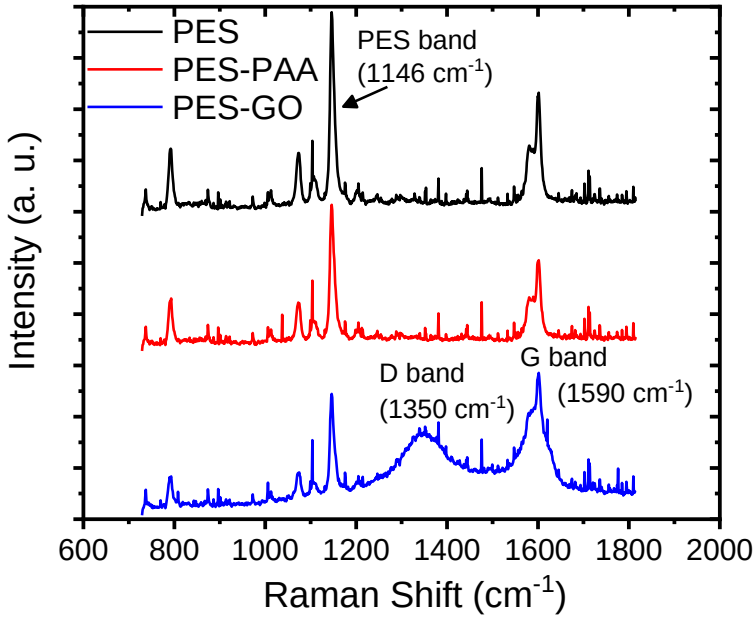

Figure 8. Raman spectra of pristine PES, PES-PAA, and PES-GO.

Spectrums of pristine PES, poly(acrylic acid) (PAA)-functionalized PES (PES-PAA), and GO-modified PES (PES-GO) substrates.

Confocal Raman mapping was used to assess the spatial distribution of GO on the PES-GO substrates. The results are presented in Fig. 9. The PES-GO map (Fig. 9 (c)) exhibits high brightness regions indicative of the presence of GO nanosheets throughout the scanned area (the intensity of each pixel is proportional to the ratio of the area under the D peak of GO to that under the polyethersulfone peak at 1146 cm^{-1}). Neither the PES nor the PES-PAA Raman maps (Fig. 9(a-b)) exhibit signatures of GO. The data in Fig. 9 shows that the modification protocol enabled the formation of uniform layers of tethered GO nanosheets on the PES substrates.

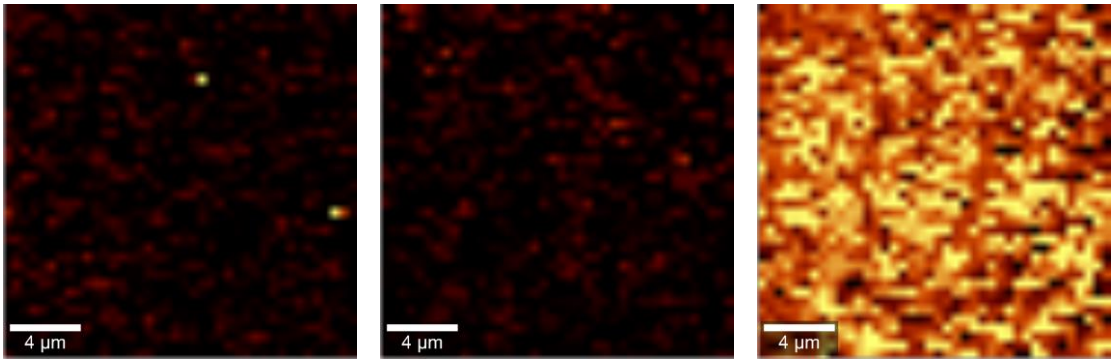

(a) **(b)** **(c)**

Figure 9. Raman spectroscopy maps of (a) pristine PES, (b) PES-PAA, and (c) PES-GO. Spectrums of pristine PES, poly(acrylic acid) (PAA)-functionalized PES (PES-PAA), and GO-modified PES (PES-GO) substrates.

Interfacial Properties

The interfacial properties known to influence biofouling propensity were investigated. These include: hydrophobicity, nanoscale roughness and surface charge [33], [83]. To characterize the hydrophobicity of each substrate type, the contact angle of *n*-decane droplets in aqueous suspension was measured using the captive bubble technique. The angles shown below are measured from the substrate, through the aqueous phase, to the *n*-decane interface, so that smaller values indicate poor wetting of the substrate by the *n*-decane droplet (i.e., greater hydrophilicity). The results, presented in Fig. 10 (a), show that PES-PAA ($\theta_{n\text{-Decane}}$ = 20.6 ± 4.3°) and PES-GO samples ($\theta_{n\text{-Decane}}$ = 19.7 ± 5.4°) were significantly more hydrophilic ($p < 0.01$) than the control PES substrate ($\theta_{n\text{-Decane}}$ = 53.1 ± 3.9°). PES-PAA and PES-GO showed approximately equivalent contact angles ($p = 0.6$). This low wettability (contact angle) of PES-AA and PES-GO surfaces by a hydrophobic liquid (*n*-decane) was attributed to the abundance of H-bonding functional groups in PAA- and GO-functionalized surfaces (-COOH groups in PES-PAA; hydroxyl, and -COOH groups in GO [75], all of which are absent in PES).

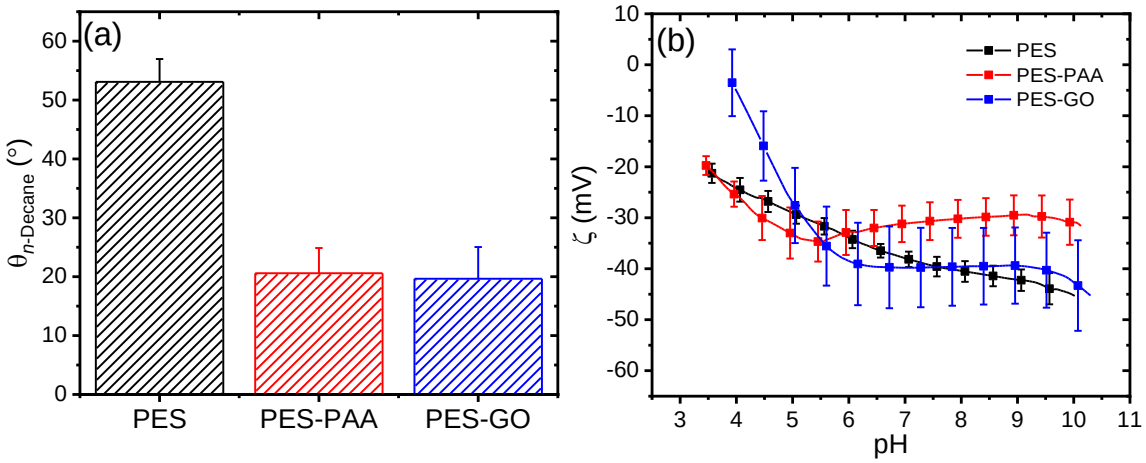

Figure 10. Contact angle and zeta potential of PES, PES-PAA, and PES-GO.

(a) Contact angles of n-decane droplets ($\theta_{n\text{-Decane}}$) on the various substrates, determined in ultrapure water via the captive bubble technique. Error bars denote one standard deviation ($n \geq 14$). (b) ζ-Potential as a function of pH of pristine PES, poly(acrylic acid) (PAA)-modified PES (PES-PAA), and GO-modified PES (PES-GO) substrates. The ζ-potential results shown for each substrate type are the average of three independently modified specimens (error bars indicate one standard deviation.

Surface Charge (Zeta Potential)

The surface charge of the substrates were characterized in terms of the ζ-potential as a function of pH. The results are presented in Fig. 10 (b). All substrates exhibited negative zeta potentials over the pH range investigated. At pH 7.4, (the conditions in which other interfacial properties were characterized such as surface roughness, and microbial adhesion), all specimens showed a similar zeta potential value of ~-30 to -40 mV. This suggests that surface functionalization did not significantly modify the charge of the interface at this pH. PES-PAA and PES-GO samples were negatively charged primarily due to deprotonation of carboxylic acid groups with increasing pH [75], [84]. While PES does not have acidic functional groups, its negative zeta potential is attributed to adsorption of hydroxyl ions [85].

Surface Roughness (AFM)

Surface roughness influences fouling, with rougher surfaces exhibiting greater biofouling and colloidal fouling propensity [35], [86]–[88]. The RMS roughness (R_{RMS}) of the hydrated substrates was determined using AFM. Representative 2 × 2 μm^2 AFM scans along with average R_{RMS} values are shown in Fig. 11. A Relatively smooth interface was observed in the PES substrate with low surface roughness (R_{RMS} = 2.51 ± 0.49 nm, Fig. 11 (a)). On the other hand, the grafted PAA chains increased the R_{RMS} of the PES-PAA substrate (R_{RMS} = 5.74 ± 2.18 nm, Fig. 11 (b)) compared to the PES control ($p < 0.01$). The negatively charged tethered PAA chains likely were in a collapsed non-extended conformation given that the high ionic strength of PBS (162 mM) would result in screening of electrostatic repulsions [89]. This PAA chain collapse yielded the rougher peak-and-valley interfacial structure shown in Fig. 11 (b). Upon edge-tethering GO nanosheets to the PAA surface, it was observed that an interface with lower R_{RMS} (R_{RMS} = 3.63 ± 1.17 nm, Fig. 11 (c)) resulted compared to PES-PAA (p = 0.03). GO nanosheets appeared to cover the rougher PAA interfacial features, thus decreasing R_{RMS}.

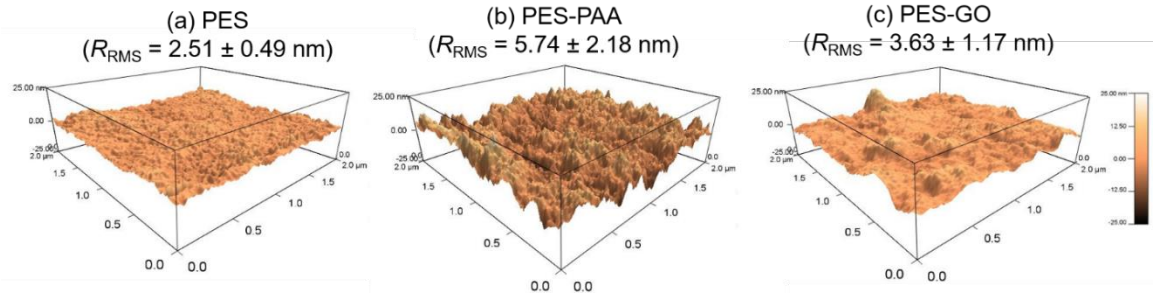

Figure 11. Surface roughness (RMS) of PES, PES-PAA, and PES-GO.

AC mode AFM images of (a) pristine PES, (b) poly(acrylic acid) (PAA)-modified PES (PES-PAA), and (c) GO-modified PES (PES-GO) substrates. The caption denotes the root-mean-squared roughness (R_{RMS}) computed from eight 1 × 1 μm2 sections sampled

over two different 5 × 5 μm2 scans of each substrate type. AFM scans and RRMS were obtained in PBS (pH 7.4).

Biocidal Activity and Bacterial Adhesion

The biocidal activity and mechanism of bacterial adhesion onto GO-functionalized substrates was investigated. First, it was determined whether PES-GO substrates exhibit cytotoxicity by counting colony-forming units (CFU) of bacteria [52], [90] using a bacterial assay. Next, single-cell force spectroscopy was used to determine whether GO substrate functionalization mitigates bacterial adhesion, the first step in biofouling, in addition to inactivating bacteria [19], [52]. GO coatings that are both biocidal and anti-adhesive are preferable to those that afford only bacterial inactivation (without preventing bacteria, and bacterial debris, from adsorbing). While previous work on GO-functionalized polyamide membranes has shown that GO coatings may exert dual biocidal/anti-adhesive functions [91], recent studies have shown that GO nanosheets increase the adhesiveness of inert Si substrates [25] and weakly adhesive polymeric spacer substrates [26]. These seemingly contradictory results are examined and explained here.

Biocidal Activity

The biocidal activity of the substrates was evaluated using a colony counting assay. The results are presented in Fig. 12, showing the number of colony forming units (CFU) normalized by the PES control. Results for PES-GO substrates indicated strong biocidal activity against *P. fluorescens*, with the number of colonies on the PES-GO surface being 8.1% of the control PES following a 1-h exposure ($p < 0.05$, one-sided unpaired *t*-test). This result is consistent with previous studies demonstrating the biocidal activity of GO films against Gram-negative (e.g., *E. coli* [18], *P. aeruginosa* [20]) and Gram-positive

bacteria (e.g., *S. aureus* [67]). While the precise mode of biocidal action of GO in bacteria is not completely understood, there is increasing evidence of the determining role of oxidative pathways [19], either mediated by GO-catalyzed generation of reactive oxygen species [54] or through direct GO oxidation of cell constituents [69], [92].

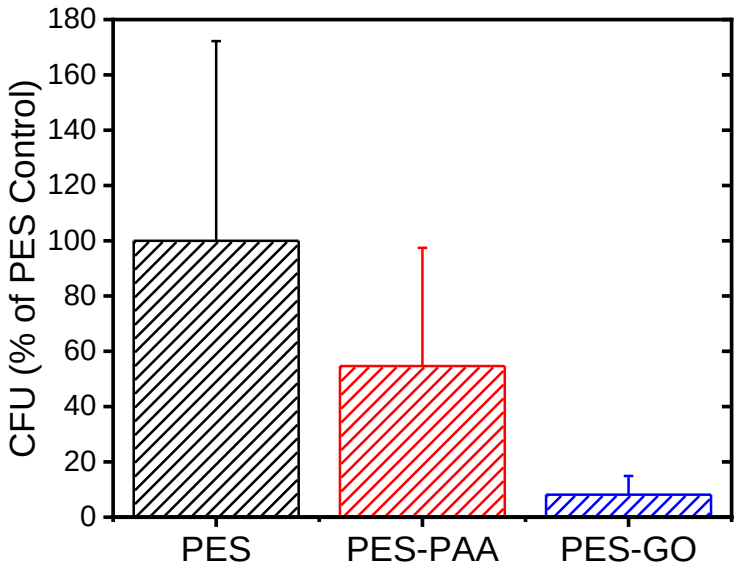

Figure 12. Biocidal assay results for PES, PES-PAA, and PES-GO.

Biocidal activity of pristine PES, poly(acrylic acid) (PAA)-modified PES (PES-PAA), and GO-modified PES (PES-GO) substrates. Colony-forming units (CFU) are shown as % of the PES control. Error bars denote the standard deviation of three experiments.

It is important to note that the CFU data in Fig. 12 are influenced by substrate adhesiveness. Thus, the lower CFU count on PES-PAA compared to PES is due to the more hydrophilic PAA coating (Fig. 10 (a)), which lowers the extent of bacterial deposition on this substrate. Meanwhile, the low CFU count on PES-GO is a result of both the intrinsic cytotoxicity of GO and the interfacial properties of PES-GO. However, the relative contributions of adhesion mitigation and biocidal activity cannot be disentangled with a simple colony counting assay.

Bacterial Adhesion

To establish the extent to which PES-GO substrates mitigate bacterial adhesion, AFM-based single-cell force spectroscopy (SCFS) was used to directly measure bacterial adhesion forces. A representative force-distance curve, showing a typical extension−retraction force cycle, is presented in Fig. 13. For each retraction force curve, the peak adhesion force, F_{Peak}, defined as the binding force with the highest magnitude, and the rupture separation, R, i.e., the separation at which cell-substrate forces vanish (Fig. 13) was recorded. The trigger force (F_{Tr}, defined as the force exerted on the bacterium when it contacts the substrate, Fig. 13), was set to 600 pN. This value is of the same order of magnitude as the permeation drag force experienced by similarly-sized colloidal particles during low-pressure membrane filtration [93]. Therefore, these measurements were performed with comparable forces to what bacteria would experience during membrane operation.

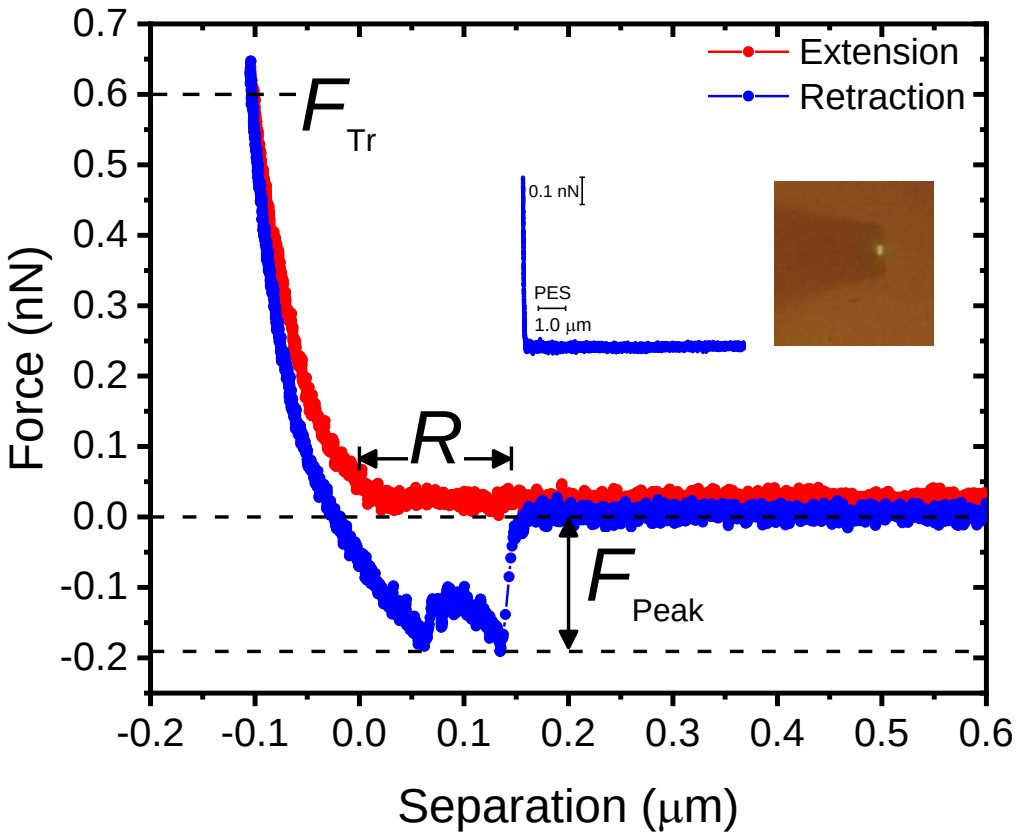

Figure 13. Representative extension-retraction force cycle recorded over PES.

Measurements recorded with a *P. fluorescens* bacterial probe. The curve shows the definition of the trigger force (F_{Tr}), peak adhesion force (F_{Peak}), and rupture separation (R). The inset shows a representative non-adhesive retraction force curve recorded over PES, and a digital image of a bacterial probe.

Fig. 14 (a-c) presents the distribution of *P. fluorescens* peak adhesion forces (F_{Peak}) observed over the different substrates. The "NO" column in the histograms corresponds to measurements in which weak adhesion (< 30 pN, equivalent in magnitude to the noise level in the force) or no adhesion peaks were observed (see Fig. 13 (inset) for a representative non-adhesive force curve).

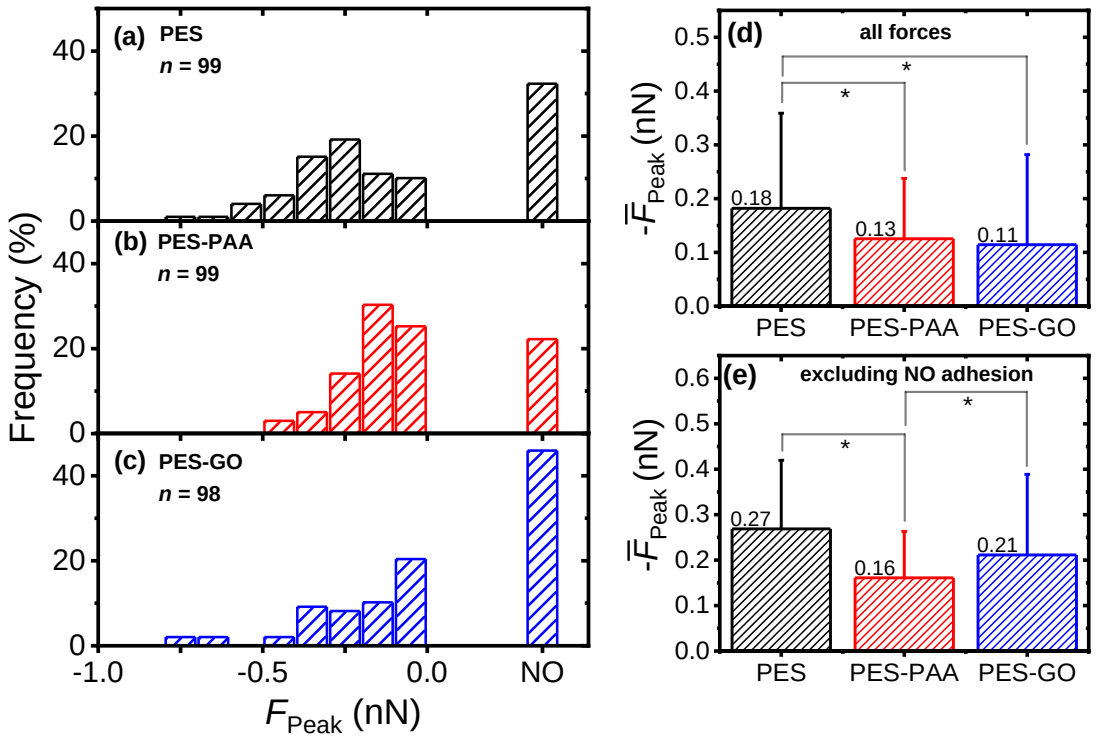

Figure 14. Distribution of peak adhesion forces (F_{Peak}) over PES, PES-PAA, and PES-GO.

Measurements performed with single *P. fluorescens* cells on: (a) pristine PES; (b) poly(acrylic acid) (PAA)-modified PES (PES-PAA); (c) GO-modified PES (PES-GO). The inset shows the number of force measurements (n). Measurements were performed in PBS at pH 7.4. (d) Mean peak adhesion forces ($\overline{F}_{Peak}$) computed from (a)-(c), including non-adhesive events (F_{Peak} = 0 nN). (e) Mean peak adhesion forces excluding non-adhesive events. Error bars in (d) and (e) indicate the standard deviation. Pairwise comparisons denoted by * indicate statistical significance ($p < 0.05$).

A broad distribution of peak adhesion forces was observed for all substrates (Fig. 14 (a)-(c)), with the majority of adhesion events occurring in the ≈ 0 to 0.5 nN range, typical of bacterial adhesion [94]. Further, it was observed that adhesion forces were substrate-dependent. Among the surfaces studied, PES-GO exhibited the lowest probability of adhesion, with 45.9% of measurements showing no-adhesion events, compared to 22.2% for PES-PAA and 32.3% for PES. Looking at the average of all adhesion forces (Fig. 14

(d)), shows that adhesion was strongest on PES ($\bar{F}_{Peak}$ = -0.18 (± 0.18) nN), while weakest on PES-GO ($\bar{F}_{Peak}$ = -0.11 (± 0.17) nN, p = 0.006). PES-PAA substrates also demonstrated weaker adhesions ($\bar{F}_{Peak}$ = -0.13 (± 0.11) nN) compared to PES (p = 0.008), while similar adhesiveness was displayed by PES-PAA and PES-GO (p = 0.6). The similar bacterial adhesion forces observed on these two substrates indicate that the lower CFU count observed for PES-GO (Fig. 12) compared to PES-PAA was primarily due to the bactericidal activity of GO.

A more nuanced adhesion behavior emerges when the non-adhesive measurements were excluded from the calculation of the mean. The results, presented in Fig. 14 (e), show that PES substrates still exhibited the strongest mean adhesion, ($\bar{F}_{Peak}$ = -0.27 (± 0.15) nN). However, PES-PAA exhibited the weakest mean adhesion forces ($\bar{F}_{Peak}$ = -0.16 (± 0.10) nN) compared to PES-GO ($\bar{F}_{Peak}$ = -0.21 (± 0.18) nN, p = 0.04). Consequently, Fig. 14 shows that, while PES-GO surfaces displayed the lowest probability of *P. fluorescens* attachment (the highest incidence of non-adhesion events, Fig. 14 (c)), adhering bacteria engaged the GO substrate with forces that were stronger than those observed over PES-PAA, and only somewhat weaker than those observed over PES (Fig. 14 (e)).

The results shown in Fig. 14 indicate that edge-tethering GO to a PAA coating decreased the mean adhesion force ($\bar{F}_{Peak}$) of *P. fluorescens* compared to the unmodified PES surface (Fig. 14 (d)), while preserving the biocidal properties of GO coatings (Fig. 12). Consequently, PES-GO surfaces exhibited simultaneous low-adhesion and biocidal activity. However, it is important to note that the lower $\bar{F}_{Peak}$ observed on PES-GO (Fig. 14 (d)) was due to a high incidence of non-adhesive events on the GO-functionalized substrate

(Fig. 14 (c)), which offsets the relatively strong adhesion forces exhibited by cells that do successfully adhere to the PES-GO surface (Fig. 14 (e)).

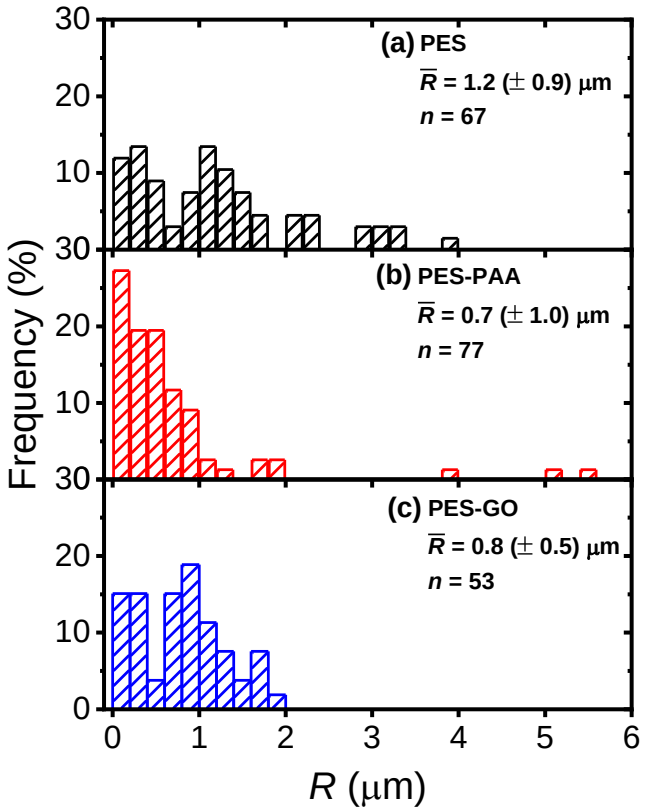

Figure 15. Distribution of rupture separations (R) over PES, PES-PAA, and PES-GO.

R defined as the distance at which cell adhesion forces vanish, for various substrates: (a) pristine PES; (b) poly(acrylic acid) (PAA)-modified PES (PES-PAA); (c) GO-modified PES (PES-GO). The inset shows the histogram average ($\bar{R}$ (± standard deviation)), and number of measurements (n). Measurements were performed in PBS at pH 7.4.

Fig. 15 presents the distribution of the rupture separation (R) over the different substrates. The rupture separations were distributed broadly, with mean values ($\bar{R}$) around 1 μm that are a reflection of the adhesins, namely pili and flagella, that mediate *P. fluorescens* binding to substrates [95]–[97]**.** Fig. 15 also shows that longer ranged interactions were observed over PES ($\bar{R}$ = 1.2 (± 0.9 μm)) compared to PES-PAA ($\bar{R}$ = 0.7 (± 1.0 μm), p = 0.002) and

to PES-GO ($\overline{\boldsymbol{R}}$ = 0.8 (± 0.5 μm), p = 0.008), suggesting that more sites along individual adhesins bound to the PES substrate. It is also possible that higher $\overline{\boldsymbol{R}}$ observed on the PES substrate indicates that several adhesins of different contour length facilitated attachment on PES [39]**.** Rupture separations thus display behavior in line with the adhesion forces reported in Fig. 14 (d), since longer ranged forces were observed on the more adhesion-prone PES substrates. Moreover, in view of the lower $\overline{\boldsymbol{R}}$ observed over PES-GO and PES-PAA, Fig. 15 shows that the range of cell adhesion forces was determined by microbial adhesins, and that extension of poly(acrylic acid) chains during cell pull-off did not contribute significantly to *R*.

Examining the interfacial properties presented in Figs. 10 and 11 allows the explanation for the differences in adhesive behavior among the three substrate types. Weakening of cell-substrate forces in PES-PAA (Fig. 14 (d-e)) compared to PES was due to the PAA coatings that resulted in more hydrophilic substrates (Fig. 10 (a)). These hydrophilic coatings would mitigate adhesion of *P. fluorescens* bacteria reliant on hydrophobic interactions [39], [95], [98]**.** In addition, PAA chain compression results in a steric repulsive force that contributes to weaker bioadhesion [99], [100]**.** It is noted that long-range electrostatic repulsive forces involving the negatively charged substrate (Fig. 10 (b)) and bacterium were absent in PBS (Debye length = 0.75 nm). Two effects were observed upon functionalization with GO. First, an increase in the frequency of non-adhesive events compared to PES and PES-PAA ("NO" column in Fig. 14 (a-c)), which was attributed to the layer of GO nanosheets covalently bound to PES-PAA. This GO coating lowered the roughness of the interface (Fig. 11) thus decreasing adsorption surface area, resulting in an additional steric barrier that limited binding of the microbe [25]**.** Similarly, the higher

surface roughness in PES-PAA explained its lower incidence of non-adhesive events compared to PES. Second, an increase in the mean adhesion force relative to PES-PAA excluding the non-adhesive events (Fig. 14 (e)) was observed. When considering the similar contact angles of PES-PAA and PES-GO (Fig. 10 (a)), the stronger adhesion on the GO-coated substrate can't be explained by a macroscopic view of hydrophobicity. At the nanoscale, however, GO is known to be amphiphilic, possessing both hydrophilic sheet edges [75]**,** and hydrophobic sheet surfaces with non-oxidized graphenic domains [75], [101]**.** These nanoscale hydrophobic regions embedded in GO serve as sorption sites for hydrophobic molecules [102]–[104]**,** and thus could bolster microbial adhesion through interactions with hydrophobic adhesins [96]**.**

Chapter 4: Conclusion and Future Work

While graphene oxide (GO) has shown strong biocidal activity, there have been conflicting reports as to whether GO can mitigate bacterial adhesion, the first step of biofilm formation and biofouling. This thesis used single-cell force spectroscopy to show that edge-tethering GO nanosheets to poly(acrylic acid) (PAA) brushes bound to polyethersulfone (PES) produces GO coatings that exhibited low *P. fluorescens* adhesion forces and significant biocidal activity. The results showed that lower mean adhesion forces observed on GO-functionalized coatings (PES-GO) were mainly due to cell-substrate repulsive (non-adhesive) forces. These forces originate from the hydrophilicity and steric repulsion from the GO-functionalized PAA layer. A significant observation is that GO is not intrinsically anti-adhesive and that its integration into a polymeric brush is essential to achieve a low-adhesion interface. GO-free PAA coatings (PES-PAA) also demonstrated lower bacterial adhesion due to their hydrophilicity. However, these coatings did not display biocidal properties. In the absence of PAA or GO, PES control substrates exhibited stronger bacterial adhesion due to their hydrophobicity.

In addition to the work presented in this thesis, analysis using polymer chain models was performed by Sara BinAhmed on the collected SCFS force curves to determine which extracellular structures (pili, flagella, outer membrane proteins, etc) mediate the adhesion process onto the substrates tested.

In total, this research has shown that graphene oxide (GO) can't be applied directly to surfaces with the intent of lowering bacterial adhesion, but must be attached using methods that exhibit additional bacterial repulsion (like hydrophilic polymer brushes) to achieve both a biocidal and anti-adhesive GO coating. Future work could focus on varying the

mechanism of GO tethering coupled with SCFS analysis to determine functionalization methods that further improve the anti-adhesive properties of GO. In addition, graphene oxide sheet sizes could be manipulated to determine its effect on bacterial adhesion.

References

[1] K. Peinemann and P. Nunes, *Further Volumes of this Series Nonporous Inorganic Membranes Materials Science of Membranes for Gas and Vapor Separation Membranen Membranes in Clean Technologies Membrane Technology and Applications*. .

[2] P. Tao, Y. Xu, and Y. Zhou, "Coal-Based Carbon Membrane Coupled with Electrochemical Oxidation Process for the Enhanced Microalgae Removal from Simulated Ballast Water," pp. 1–8, 2017.

[3] R. H. Peiris, M. Jaklewicz, H. Budman, R. L. Legge, and C. Moresoli, "Assessing the role of feed water constituents in irreversible membrane fouling of pilot-scale ultrafiltration drinking water treatment systems," *Water Res.*, vol. 47, no. 10, pp. 3364–3374, 2013.

[4] W. Gao *et al.*, "Membrane fouling control in ultrafiltration technology for drinking water production: A review," *Desalination*, vol. 272, no. 1–3, pp. 1–8, 2011.

[5] P. J. J. Alvarez, C. K. Chan, M. Elimelech, N. J. Halas, and D. Villagrán, "Emerging opportunities for nanotechnology to enhance water security," *Nat. Nanotechnol.*, vol. 13, no. 8, pp. 634–641, 2018.

[6] A. Figoli, *Green Chemistry and Sustainable Technology Sustainable Membrane Technology for Water and Wastewater Treatment*. .

[7] G. dong Kang and Y. ming Cao, "Development of antifouling reverse osmosis membranes for water treatment: A review," *Water Res.*, vol. 46, no. 3, pp. 584–600, 2012.

[8] A. Matin, Z. Khan, S. M. J. Zaidi, and M. C. Boyce, "Biofouling in reverse osmosis membranes for seawater desalination: Phenomena and prevention," *Desalination*, vol. 281, no. 1, pp. 1–16, 2011.

[9] C. S. Ong, P. S. Goh, W. J. Lau, N. Misdan, and A. F. Ismail, "Nanomaterials for biofouling and scaling mitigation of thin fi lm composite membrane : A review," *DES*, vol. 393, pp. 2–15, 2016.

[10] M. Bagheri and S. Ahmad, "Bioresource Technology Critical review of fouling mitigation strategies in membrane bioreactors treating water and wastewater," *Bioresour. Technol.*, vol. 258, no. January, pp. 318–334, 2018.

[11] S. I. Patsios, T. B. Goudoulas, E. G. Kastrinakis, S. G. Nychas, and A. J. Karabelas, "A novel method for rheological characterization of biofouling layers developing in Membrane Bioreactors (MBR)," *J. Memb. Sci.*, vol. 482, pp. 13–24, 2015.

[12] T. Mbr, "Wastewater recycling to potable water standards," no. October, pp. 38–40, 2010.

[13] O. Habimana, A. J. C. Semião, and E. Casey, "The role of cell-surface interactions in bacterial initial adhesion and consequent bio fi lm formation on nano fi ltration /

reverse osmosis membranes," *J. Memb. Sci.*, vol. 454, pp. 82–96, 2014.

[14] D. Lee, Y. Lee, S. S. Choi, S. H. Lee, K. W. Kim, and Y. Lee, "Effect of membrane property and feed water organic matter quality on long-term performance of the gravity-driven membrane filtration process," *Environ. Sci. Pollut. Res.*, pp. 1–11, 2017.

[15] V. Kochkodan and N. Hilal, "A comprehensive review on surface modi fi ed polymer membranes for biofouling mitigation," *DES*, vol. 356, pp. 187–207, 2015.

[16] C. X. Liu, D. R. Zhang, Y. He, X. S. Zhao, and R. Bai, "Modification of membrane surface for anti-biofouling performance : Effect of anti-adhesion and anti-bacteria approaches," vol. 346, pp. 121–130, 2010.

[17] J. Chen, H. Peng, X. Wang, F. Shao, Z. Yuan, and H. Han, "Graphene oxide exhibits broad-spectrum antimicrobial activity against bacterial phytopathogens and fungal conidia by intertwining and membrane perturbation," *Nanoscale*, vol. 6, no. 3, pp. 1879–1889, 2014.

[18] W. Hu *et al.*, "Graphene-based antibacterial paper," *ACS Nano*, vol. 4, no. 7, pp. 4317–4323, 2010.

[19] F. Perreault, A. F. De Faria, S. Nejati, and M. Elimelech, "Antimicrobial Properties of Graphene Oxide Nanosheets: Why Size Matters," *ACS Nano*, vol. 9, no. 7, pp. 7226–7236, 2015.

[20] S. Gurunathan, J. W. Han, A. A. Dayem, V. Eppakayala, and J. H. Kim, "Oxidative stress-mediated antibacterial activity of graphene oxide and reduced graphene oxide in Pseudomonas aeruginosa," *Int. J. Nanomedicine*, vol. 7, pp. 5901–5914, 2012.

[21] H. R. Chae, J. Lee, C. H. Lee, I. C. Kim, and P. K. Park, "Graphene oxide-embedded thin-film composite reverse osmosis membrane with high flux, anti-biofouling, and chlorine resistance," *J. Memb. Sci.*, vol. 483, pp. 128–135, 2015.

[22] M. E. A. Ali, L. Wang, X. Wang, and X. Feng, "Thin film composite membranes embedded with graphene oxide for water desalination," *Desalination*, vol. 386, pp. 67–76, 2016.

[23] A. Inurria *et al.*, "Polyamide thin-film nanocomposite membranes with graphene oxide nanosheets: Balancing membrane performance and fouling propensity," *Desalination*, vol. 451, pp. 139–147, 2018.

[24] X. Lu, X. Feng, X. Zhang, M. N. Chukwu, C. O. Osuji, and M. Elimelech, "Fabrication of a Desalination Membrane with Enhanced Microbial Resistance through Vertical Alignment of Graphene Oxide," *Environ. Sci. Technol. Lett.*, vol. 5, no. 10, pp. 614–620, 2018.

[25] J. Xue, S. Binahmed, Z. Wang, N. G. Karp, B. L. Stottrup, and S. R. Castrillo, "Bacterial Adhesion to Graphene Oxide (GO) -Functionalized Interfaces Is Determined by Hydrophobicity and GO Sheet Spatial Orientation," 2018.

[26] D. Rice, A. C. Barrios, Z. Xiao, A. Bogler, E. Bar-Zeev, and F. Perreault, "Development of anti-biofouling feed spacers to improve performance of reverse osmosis modules," *Water Res.*, vol. 145, pp. 599–607, 2018.

[27] A. Jawor and E. M. V Hoek, "Effects of feed water temperature on inorganic fouling of brackish water RO membranes," *DES*, vol. 235, no. 1–3, pp. 44–57, 2009.

[28] W. Guo, H. Ngo, and J. Li, "Bioresource Technology A mini-review on membrane fouling," *Bioresour. Technol.*, vol. 122, pp. 27–34, 2012.

[29] A. L. Lim and R. Bai, "Membrane fouling and cleaning in microfiltration of activated sludge wastewater," vol. 216, pp. 279–290, 2003.

[30] A. Al, M. Sadrzadeh, R. Chatterjee, S. Bhattacharjee, and S. De, "Colloidal fouling of nano fi ltration membranes : A novel transient electrokinetic model and experimental study," vol. 138, pp. 153–163, 2015.

[31] G. Mustafa, K. Wyns, A. Buekenhoudt, and V. Meynen, "New insights into the fouling mechanism of dissolved organic matter applying nano fi ltration membranes with a variety of surface chemistries," *Water Res.*, vol. 93, pp. 195–204, 2016.

[32] D. M. Owen, G. L. Amy, Z. K. Chowdhury, R. Paode, G. Mccoy, and K. Viscosil, "characterization and treatability," no. C, pp. 46–63, 1995.

[33] A. Weis, M. R. Bird, M. Nyström, and C. Wright, "The influence of morphology, hydrophobicity and charge upon the long-term performance of ultrafiltration membranes fouled with spent sulphite liquor," *Desalination*, vol. 175, no. 1 SPEC. ISS., pp. 73–85, 2005.

[34] T. Nguyen, F. A. Roddick, and L. Fan, "Biofouling of water treatment membranes: A review of the underlying causes, monitoring techniques and control measures," *Membranes (Basel).*, vol. 2, no. 4, pp. 804–840, 2012.

[35] M. Pasmore *et al.*, "Effects of ultrafiltration membrane surface properties on Pseudomonas aeruginosa biofilm initiation for the purpose of reducing biofouling," *J. Memb. Sci.*, vol. 194, no. 1, pp. 15–32, 2001.

[36] K. Zodrow *et al.*, "Polysulfone ultrafiltration membranes impregnated with silver nanoparticles show improved biofouling resistance and virus removal," *Water Res.*, vol. 43, no. 3, pp. 715–723, 2009.

[37] M. Homayoonfal, A. Akbari, and M. R. Mehrnia, "Preparation of polysulfone nanofiltration membranes by UV-assisted grafting polymerization for water softening," *Desalination*, vol. 263, no. 1–3, pp. 217–225, 2010.

[38] S. T. Kang, A. Subramani, E. M. V. Hoek, M. A. Deshusses, and M. R. Matsumoto, "Direct observation of biofouling in cross-flow microfiltration: Mechanisms of deposition and release," *J. Memb. Sci.*, vol. 244, no. 1–2, pp. 151–165, 2004.

[39] S. Binahmed, A. Hasane, Z. Wang, A. Mansurov, and S. Romero-Vargas Castrillón, “Bacterial Adhesion to Ultrafiltration Membranes: Role of Hydrophilicity, Natural Organic Matter, and Cell-Surface Macromolecules,” *Environ. Sci. Technol.*, vol. 52, no. 1, pp. 162–172, 2018.

[40] T. Roger, M. Bhakoo, and Z. Zhang, “Bacterial adhesion and biofilms on surfaces,” vol. 18, pp. 1049–1056, 2008.

[41] S. Binahmed, A. Hasane, Z. Wang, A. Mansurov, and S. R. Castrillo, “Bacterial Adhesion to Ultra fi ltration Membranes : Role of Hydrophilicity , Natural Organic Matter , and Cell-Surface Macromolecules,” 2018.

[42] B. Gao, X. Zhu, C. Xu, Q. Yue, W. Li, and J. Wei, “Influence of extracellular polymeric substances on microbial activity and cell hydrophobicity in biofilms,” vol. 232, no. October 2007, pp. 227–232, 2008.

[43] J. Wingender, T.r. Neu, H.-C. Flemming (Eds.), "Microbial Extracellular Polymeric Substances, Characterization, Structure and Function," *Springer,* 1999

[44] W. Cai and Y. Liu, “Enhanced membrane biofouling potential by on-line chemical cleaning in membrane bioreactor,” *J. Memb. Sci.*, vol. 511, pp. 84–91, 2016.

[45] J. Yin, Y. Yang, Z. Hu, and B. Deng, “Attachment of silver nanoparticles (AgNPs) onto thin- fi lm composite (TFC) membranes through covalent bonding to reduce membrane biofouling,” *J. Memb. Sci.*, vol. 441, pp. 73–82, 2013.

[46] A. Soroush, W. Ma, M. Cyr, S. Rahaman, B. Asadishad, and N. Tufenkji, “In Situ Silver Decoration on Graphene Oxide-Treated Thin Film Composite Forward Osmosis Membranes : Biocidal Properties and Regeneration Potential,” pp. 3–8, 2016.

[47] C. Thamaraiselvan, Y. Carmiel, G. Eliad, C. N. Sukenik, R. Semiat, and C. G. Dosoretz, “Modi fi cation of a polypropylene feed spacer with metal oxide-thin fi lm by chemical bath deposition for biofouling control in membrane fi ltration,” *J. Memb. Sci.*, vol. 573, no. December 2018, pp. 511–519, 2019.

[48] W. Ma *et al.*, “Spray- and spin-assisted layer-by-layer assembly of copper nanoparticles on thin- fi lm composite reverse osmosis membrane for biofouling mitigation,” *Water Res.*, vol. 99, pp. 188–199, 2016.

[49] J. Huang, H. Wang, and K. Zhang, “Modi fi cation of PES membrane with Ag – SiO 2 : Reduction of biofouling and improvement of fi ltration performance,” vol. 336, pp. 8–17, 2014.

[50] A. V. Dudchenko, J. Rolf, K. Russell, W. Duan, and D. Jassby, “Organic fouling inhibition on electrically conducting carbon nanotube – polyvinyl alcohol composite ultra filtration membranes,” *J. Memb. Sci.*, vol. 468, pp. 1–10, 2014.

[51] E. Igbinigun, Y. Fennell, R. Malaisamy, K. L. Jones, and V. Morris, “Graphene oxide functionalized polyethersulfone membrane to reduce organic fouling,” *J. Memb. Sci.*, vol. 514, pp. 518–526, 2016.

[52] F. Perreault, M. E. Tousley, and M. Elimelech, “Thin-Film Composite Polyamide Membranes Functionalized with Biocidal Graphene Oxide Nanosheets,” *Environ. Sci. Technol. Lett.*, vol. 1, no. 1, pp. 71–76, 2013.

[53] S. Y. Lee, H. J. Kim, R. Patel, S. J. Im, J. H. Kim, and B. R. Min, “Silver nanoparticles immobilized on thin film composite polyamide membrane : characterization , nanofiltration , antifouling properties,” no. April, pp. 562–568, 2007.

[54] Y. Zhang *et al.*, “Cytotoxicity effects of graphene and single-wall carbon nanotubes in neural phaeochromocytoma-derived pc12 cells,” *ACS Nano*, vol. 4, no. 6, pp. 3181–3186, 2010.

[55] Y. Zhu *et al.*, “Graphene and graphene oxide: Synthesis, properties, and applications,” *Adv. Mater.*, vol. 22, no. 35, pp. 3906–3924, 2010.

[56] E. Science and T. Letters, “Supporting Information Thin-Film Composite Polyamide Membranes Functionalized with Biocidal Graphene Oxide Nano sheets,” no. 203.

[57] R. K. Joshi *et al.*, “Precise and ultrafast molecular sieving through graphene oxide membranes,” *Science (80-.).*, vol. 343, no. 6172, pp. 752–754, 2014.

[58] S. C. O’Hern *et al.*, “Selective ionic transport through tunable subnanometer pores in single-layer graphene membranes,” *Nano Lett.*, vol. 14, no. 3, pp. 1234–1241, 2014.

[59] M. Hu and B. Mi, “Enabling graphene oxide nanosheets as water separation membranes,” *Environ. Sci. Technol.*, vol. 47, no. 8, pp. 3715–3723, 2013.

[60] N. Yousefi, X. Lu, M. Elimelech, and N. Tufenkji, “Environmental performance of graphene-based 3D macrostructures,” *Nat. Nanotechnol.*, 2018.

[61] X. Wang, Y. Zhao, E. Tian, J. Li, and Y. Ren, “Graphene Oxide-Based Polymeric Membranes for Water Treatment,” vol. 1701427, pp. 1–20, 2018.

[62] S. Nasseri, S. Ebrahimi, M. Abtahi, and R. Saeedi, “Synthesis and characterization of polysulfone / graphene oxide nano- composite membranes for removal of bisphenol A from water,” *J. Environ. Manage.*, vol. 205, pp. 174–182, 2018.

[63] J. Zhang, Z. Xu, M. Shan, B. Zhou, Y. Li, and B. Li, “Synergetic effects of oxidized carbon nanotubes and graphene oxide on fouling control and anti-fouling mechanism of polyvinylidene fl uoride ultra fi ltration membranes,” *J. Memb. Sci.*, vol. 448, pp. 81–92, 2013.

[64] N. Ahmad, A. Kausar, and B. Muhammad, “An investigation on 4-aminobenzoic acid modified polyvinyl chloride / graphene oxide and PVC / graphene oxide based nanocomposite membranes,” 2016.

[65] A. F. Ismail, M. Padaki, N. Hilal, T. Matsuura, and W. J. Lau, “Thin fi lm composite membrane — Recent development and future potential,” *DES*, vol. 356, pp. 140–148, 2015.

[66] Y. Wei, Y. Zhang, X. Gao, Z. Ma, and X. Wang, “Multilayered graphene oxide membranes for water treatment : A review,” *Carbon N. Y.*, vol. 139, no. 238, pp. 964–981, 2018.

[67] O. Akhavan and E. Ghaderi, “Toxicity of Graphene and Graphene Oxide Nanowalls Against Bacteria,” vol. 4, no. 10, pp. 5731–5736, 2010.

[68] P. K. S. Mural, S. Jain, S. Kumar, G. Madras, and S. Bose, “graphene oxide sheets anchored on to 3D porous,” pp. 8048–8057, 2016.

[69] S. Liu, T. H. Zeng, M. Hofmann, E. Burcombe, J. Wei, and R. Jiang, “Antibacterial Activity of Graphite , Graphite Oxide , Graphene Oxide , and Reduced Graphene Oxide : Membrane and Oxidative Stress,” no. 9, pp. 6971–6980, 2011.

[70] Q. Huang, C. Fan, H. Fang, and R. Zhou, “Destructive extraction of phospholipids from Escherichia coli membranes by graphene nanosheets,” *Nat. Nanotechnol.*, vol. 8, no. 8, pp. 594–601, 2013.

[71] J. Helenius, C. Heisenberg, H. E. Gaub, and D. J. Muller, “Single-cell force spectroscopy,” 2008.

[72] H. Wang and H. R. Brown, “Self-initiated photopolymerization and photografting of acrylic monomers,” *Macromol. Rapid Commun.*, 2004.

[73] J. Deng, L. Wang, L. Liu, and W. Yang, “Developments and new applications of UV-induced surface graft polymerizations,” *Prog. Polym. Sci.*, 2009.

[74] B. Van Der Bruggen, “Chemical modification of polyethersulfone nanofiltration membranes: A review,” *J. Appl. Polym. Sci.*, vol. 114, no. 1, pp. 630–642, 2009.

[75] V. C. Sanchez, A. Jachak, R. H. Hurt, and A. B. Kane, “Biological interactions of graphene-family nanomaterials: An interdisciplinary review,” *Chem. Res. Toxicol.*, vol. 25, no. 1, pp. 15–34, 2012.

[76] K. N. Kudin, B. Ozbas, H. C. Schniepp, R. K. Prud’homme, I. A. Aksay, and R. Car, “Raman spectra of graphite oxide and functionalized graphene sheets,” *Nano Lett.*, vol. 8, no. 1, pp. 36–41, 2008.

[77] Z. Grabarek and J. Gergely, “Zero-length crosslinking procedure with the use of active esters,” *Anal. Biochem.*, vol. 185, no. 1, pp. 131–135, 1990.

[78] S. L. Walker, S. Bhattacharjee, E. M. V. Hoek, and M. Elimelech, “A novel asymmetric clamping cell for measuring streaming potential of flat surfaces,” *Langmuir*, vol. 18, no. 6, pp. 2193–2198, 2002.

[79] H. Ma, R. H. Davis, and C. N. Bowman, “Novel sequential photoinduced living graft polymerization,” *Macromolecules*, vol. 33, no. 2, pp. 331–335, 2000.

[80] C. Klaysom, B. P. Ladewig, G. Q. M. Lu, and L. Wang, “Preparation and characterization of sulfonated polyethersulfone for cation-exchange membranes,” *J. Memb. Sci.*, vol. 368, no. 1–2, pp. 48–53, 2011.

[81] E. Pretsch, P. Bühlmann, and C. Affolter, *Structure Determination of Organic Compounds*, Third Ed. Springer, 2000.

[82] L. Wang, X. Song, T. Wang, S. Wang, Z. Wang, and C. Gao, "Fabrication and characterization of polyethersulfone/carbon nanotubes (PES/CNTs) based mixed matrix membranes (MMMs) for nanofiltration application," *Appl. Surf. Sci.*, vol. 330, pp. 118–125, 2015.

[83] P. J. Evans, M. R. Bird, A. Pihlajamäki, and M. Nyström, "The influence of hydrophobicity, roughness and charge upon ultrafiltration membranes for black tea liquor clarification," *J. Memb. Sci.*, vol. 313, no. 1–2, pp. 250–262, 2008.

[84] D. Li, M. B. Müller, S. Gilje, R. B. Kaner, and G. G. Wallace, "Processable aqueous dispersions of graphene nanosheets," *Nat. Nanotechnol.*, vol. 3, no. 2, pp. 101–105, 2008.

[85] S. Kasemset, Z. He, D. J. Miller, B. D. Freeman, and M. M. Sharma, "Effect of polydopamine deposition conditions on polysulfone ultrafiltration membrane properties and threshold flux during oil/water emulsion filtration," *Polymer (Guildf).*, vol. 97, pp. 247–257, 2016.

[86] N. Park, B. Kwon, I. S. Kim, and J. Cho, "Biofouling potential of various NF membranes with respect to bacteria and their soluble microbial products (SMP): Characterizations, flux decline, and transport parameters," *J. Memb. Sci.*, vol. 258, no. 1–2, pp. 43–54, 2005.

[87] E. M. Vrijenhoek, S. Hong, and M. Elimelech, "Influence of membrane surface properties on initial rate of colloidal fouling of reverse osmosis and nanofiltration membranes," *J. Memb. Sci.*, vol. 188, no. 1, pp. 115–128, 2001.

[88] M. Elimelech, X. Zhu, A. E. Childress, and S. Hong, "Role of membrane surface morphology in colloidal fouling of cellulose acetate and composite aromatic polyamide reverse osmosis membranes," *J. Memb. Sci.*, vol. 127, no. 1, pp. 101–109, 1997.

[89] T. Wu, P. Gong, I. Szleifer, P. Vlček, V. Šubr, and J. Genzer, "Behavior of surface-anchored poly(acrylic acid) brushes with grafting density gradients on solid substrates: 1. Experiment," *Macromolecules*, vol. 40, no. 24, pp. 8756–8764, 2007.

[90] X. Lu *et al.*, "Enhanced antibacterial activity through the controlled alignment of graphene oxide nanosheets," *Proc. Natl. Acad. Sci.*, p. 201710996, 2017.

[91] F. Perreault, H. Jaramillo, M. Xie, M. Ude, L. D. Nghiem, and M. Elimelech, "Biofouling Mitigation in Forward Osmosis Using Graphene Oxide Functionalized Thin-Film Composite Membranes," *Environ. Sci. Technol.*, vol. 50, no. 11, pp. 5840–5848, 2016.

[92] X. Lu *et al.*, "Enhanced antibacterial activity through the controlled alignment of graphene oxide nanosheets," *Proc. Natl. Acad. Sci.*, p. DOI:10.1073/pnas.1710996114, Oct. 2017.

[93] A. Ronen, W. Duan, I. Wheeldon, S. Walker, and D. Jassby, “Microbial Attachment Inhibition through Low-Voltage Electrochemical Reactions on Electrically Conducting Membranes,” *Environ. Sci. Technol.*, vol. 49, no. 21, pp. 12741–12750, 2015.

[94] S. El-Kirat-Chatel, A. Beaussart, C. D. Boyd, G. A. O’Toole, and Y. F. Dufreîne, “Single-cell and single-molecule analysis deciphers the localization, adhesion, and mechanics of the biofilm adhesin LapA,” *ACS Chem. Biol.*, vol. 9, no. 2, pp. 485–494, 2014.

[95] G. Zeng, T. Müller, and R. L. Meyer, “Single-cell force spectroscopy of bacteria enabled by naturally derived proteins,” *Langmuir*, 2014.

[96] S. J. Vesper, “Production of Pili (Fimbriae) by Pseudomonas fluorescens and Correlation with Attachment to Corn Roots.,” *Appl. Environ. Microbiol.*, vol. 53, no. 7, pp. 1397–405, 1987.

[97] N. Dasgupta, S. K. Arora, and R. Ramphal, “The Flagellar System of Pseudomonas aeruginosa BT - Pseudomonas: Volume 1 Genomics, Life Style and Molecular Architecture,” J.-L. Ramos, Ed. Boston, MA: Springer US, 2004, pp. 675–698.

[98] Y. L. Ong, A. Razatos, G. Georgiou, and M. M. Sharma, “Adhesion forces between E. coli bacteria and biomaterial surfaces,” *Langmuir*, vol. 15, no. 8, pp. 2719–2725, 1999.

[99] S. Pasche, M. Textor, L. Meagher, N. D. Spencer, and H. J. Griesser, “Relationship between interfacial forces measured by colloid-probe atomic force microscopy and protein resistance of poly(ethylene glycol)-grafted poly(L-lysine) adlayers on niobia surfaces,” *Langmuir*, vol. 21, no. 14, pp. 6508–6520, 2005.

[100] S. Gon, K. N. Kumar, K. Nüsslein, and M. M. Santore, “How bacteria adhere to brushy PEG surfaces: Clinging to flaws and compressing the brush,” *Macromolecules*, vol. 45, no. 20, pp. 8373–8381, 2012.

[101] K. Erickson, R. Erni, Z. Lee, N. Alem, W. Gannett, and A. Zettl, “Determination of the local chemical structure of graphene oxide and reduced graphene oxide,” *Adv. Mater.*, vol. 22, no. 40, pp. 4467–4472, 2010.

[102] L. J. Cote, J. Kim, V. C. Tung, J. Luo, F. Kim, and J. Huang, “Graphene oxide as surfactant sheets,” *Pure Appl. Chem.*, vol. 83, no. 1, 2010.

[103] J. Kim, L. J. Cote, F. Kim, W. Yuan, K. R. Shull, and J. Huang, “Graphene oxide sheets at interfaces,” *J. Am. Chem. Soc.*, vol. 132, no. 23, pp. 8180–8186, 2010.

[104] Z. Liu, J. T. Robinson, X. Sun, and H. Dai, “PEGylated nanographene oxide for delivery of water-insoluble cancer drugs,” *J. Am. Chem. Soc.*, vol. 130, no. 33, pp. 10876–10877, 2008.

[105] A. Bouchoux, H. Roux-de Balmann, and F. Lutin, “Investigation of nanofiltration as a purification step for lactic acid production processes based on conventional and bipolar electrodialysis operations,” *Sep. Purif. Technol.*, vol. 52, no. 2, pp.

266–273, 2006.

[106] V. T. Do, C. Y. Tang, M. Reinhard, and J. O. Leckie, “Effects of hypochlorous acid exposure on the rejection of salt, polyethylene glycols, boron and arsenic(V) by nanofiltration and reverse osmosis membranes,” *Water Res.*, vol. 46, no. 16, pp. 5217–5223, 2012.

Appendix A: Supporting Information

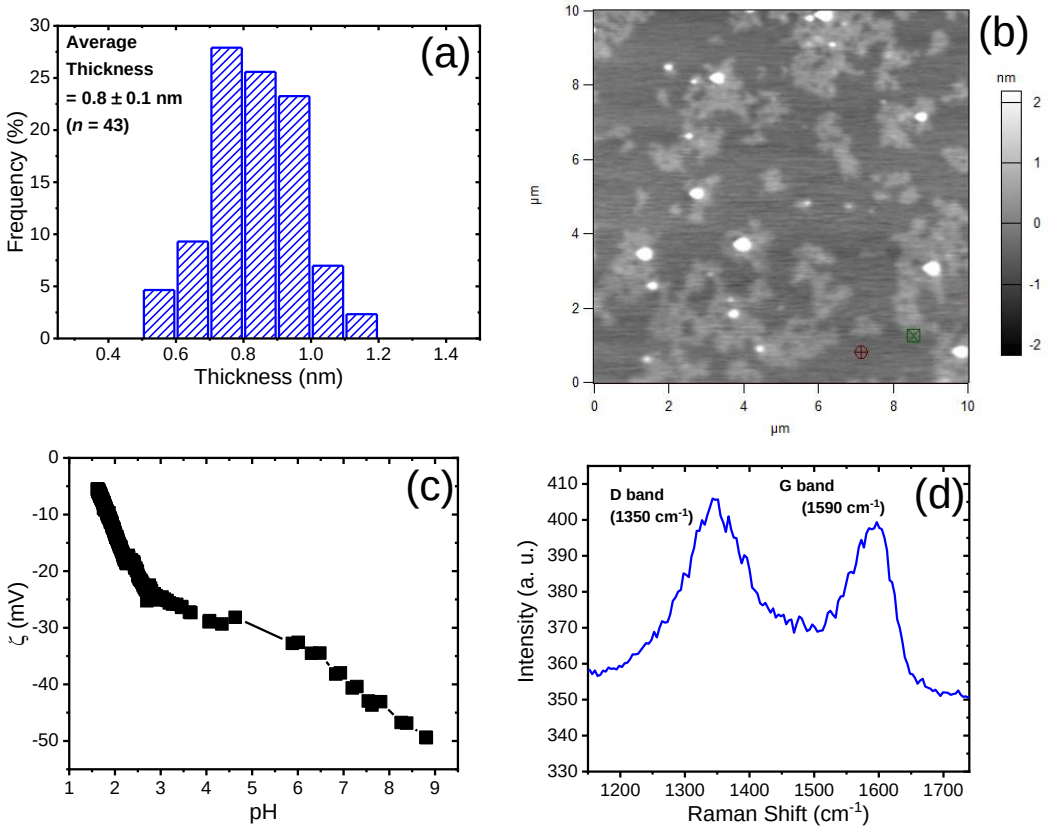

Figure S1. Characterization of graphene oxide (GO) nanosheets.

(a) distribution of nanosheet thickness determined by AC mode AFM in air using an AC160TS-R3 Si cantilever (Olympus) with nominal spring constant 26 N m^{-1} and resonance frequency 300 Hz; (b) representative AFM image of GO nanosheets deposited on a Si substrate; (c) ζ-Potential of GO in aqueous dispersion at a concentration of 250 µg mL^{-1}, determined with a Stabino zeta potential analyzer; (d) Raman spectrum of GO nanosheets deposited on a silicon wafer.

Characterization of Membrane Transport Properties

The water permeability coefficient (A) of the membranes was determined in a laboratory-scale filtration apparatus equipped with a crossflow cell (CF042D, Sterlitech, with active membrane area, A_m, of 42.1 cm^2), pump (HydraCell M-03S, Wanner Engineering), and temperature-controlled stainless steel feed reservoir. Membranes were compacted with a distilled water feed for 24 hours at a transmembrane pressure difference (Δp) of 50 psi and crossflow velocity of 0.08 m s^{-1}. Following compaction, measurements of the steady-state permeate flow rate were recorded every second for 1 hour at Δp = 50 psi and 20 °C with a digital flow meter (SLI, Sensirion). The average permeate flow rate, Q_p, was used to compute the water permeability coefficient from $A = Q_p/(A_{m\Delta}p)$. For control polyethersulfone (PES) membranes, the flux through the membranes was determined by weighing the permeate, since the permeate flow rate exceeded the maximum flow rate measurable with the digital flow meter. Four poly(acrylic acid)-modified (PES-PAA), four GO-modified (PES-GO) and two control PES membranes were characterized.

Effect of Surface Functionalization on Water Permeability and Ion Rejection

Surface modification of the PES membranes resulted in additional hydraulic resistance that decreased the water permeability coefficient (A). For pristine PES we find A = 102.1 ± 3.5 L m^{-2} h^{-1} bar^{-1}. On the other hand, for PES-PAA membranes (prepared by acrylic acid polymerization with 10-s UV exposure), we find A = 9.0 ± 1.8 L m^{-2} h^{-1} bar^{-1}, while for PES-GO, A = 7.0 ± 0.7 L m^{-2} h^{-1} bar^{-1}, i.e., the covalently bonded GO layer further decreases water permeability. We also determined the Na_2SO_4 rejection coefficient (R) at Δp = 50 psi (feed concentration = 10 mM) for the functionalized membranes using a conductivity

probe, finding R = 21.4% and 42.7% for PES-GO and PES-PAA, respectively. The A coefficient and ion rejection of PES-PAA and PES-GO materials are similar to those of nanofiltration membranes [105], [106]. Additional experiments with PES-PAA membranes prepared with 20-60 sec UV irradiation resulted in steep loss in water permeability (results not shown), due to the formation of a dense PAA layer (observe the prominent carboxyl band at 1700 cm^{-1} when the irradiation time was $\geq$ 20 s, Fig. 6).